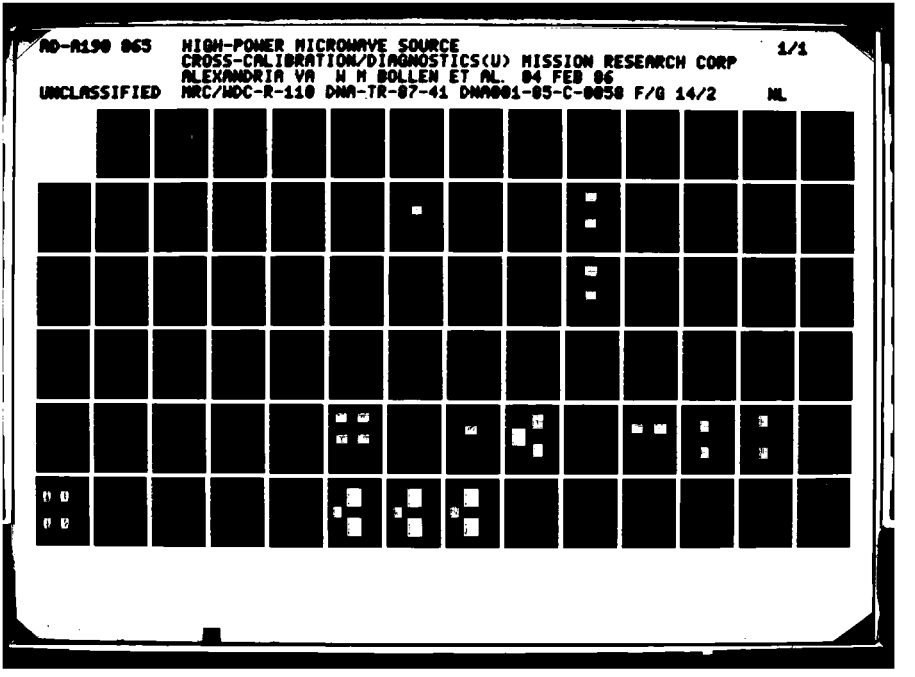
AD-A190 065
HIGH-POWER MICROWAVE SOURCE CROSS-CALIBRATION/DIAGNOSTICS(U) MISSION RESEARCH CORP ALEXANDRIA VA W H BOLLEN ET AL. 04 FEB 86
1/1
UNCLASSIFIED
MRC/WDC-R-110 DNA-TR-87-41 DNA001-85-C-0058 F/G 14/2
NL

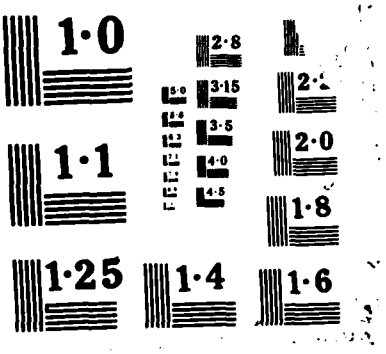
1·0
1·1
1·25
2·8
3·15
3·5
4·0
4·5
2·0
1·8
1·4
1·6

DNA-TR-87-41

HIGH-POWER MICROWAVE SOURCE CROSS-CALIBRATION/DIAGNOSTICS

W. M. Bollen
J. M. Bulson
Mission Research Corporation
5503 Cherokee Avenue, Suite 201
Alexandria, VA 22312

4 February 1986

Technical Report

CONTRACT No. DNA 001-85-C-0058

THIS WORK WAS SPONSORED BY THE DEFENSE NUCLEAR AGENCY
UNDER RDT&E RMC CODE B3460764662 RX RF 00002 25904D.

Prepared for
Director
DEFENSE NUCLEAR AGENCY
Washington, DC 20305-1000

Destroy this report when it is no longer needed. Do not return to sender.

PLEASE NOTIFY THE DEFENSE NUCLEAR AGENCY ATTN: TITL, WASHINGTON, DC 20305 1000, IF YOUR ADDRESS IS INCORRECT, IF YOU WISH IT DELETED FROM THE DISTRIBUTION LIST, OR IF THE ADDRESSEE IS NO LONGER EMPLOYED BY YOUR ORGANIZATION.

DISTRIBUTION LIST UPDATE

This mailer is provided to enable DNA to maintain current distribution lists for reports. We would appreciate your providing the requested information.

☐ Add the individual listed to your distribution list.

☐ Delete the cited organization/individual.

☐ Change of address.

NAME: _____

ORGANIZATION: _____

OLD ADDRESS	CURRENT ADDRESS
_____	_____
_____	_____
_____	_____

TELEPHONE NUMBER: ( ) _____

SUBJECT AREA(s) OF INTEREST:

_____ _____

_____ _____

_____ _____

DNA OR OTHER GOVERNMENT CONTRACT NUMBER: _____

CERTIFICATION OF NEED-TO-KNOW BY GOVERNMENT SPONSOR (if other than DNA):

SPONSORING ORGANIZATION: _____

CONTRACTING OFFICER OR REPRESENTATIVE: _____

SIGNATURE: _____

CUT HERE AND RETURN

Director
Defense Nuclear Agency
ATTN: [redacted] TITL
Washington, DC 20305-1000

Director
Defense Nuclear Agency
ATTN: [redacted] TITL
Washington, DC 20305-1000

UNCLASSIFIED
SECURITY CLASSIFICATION OF THIS PAGE

AD-A190865

REPORT DOCUMENTATION PAGE

1a REPORT SECURITY CLASSIFICATION UNCLASSIFIED	1b RESTRICTIVE MARKINGS
2a SECURITY CLASSIFICATION AUTHORITY N/A since Unclassified	3 DISTRIBUTION/AVAILABILITY OF REPORT Approved for public release; distribution is unlimited.
2b DECLASSIFICATION/DOWNGRADING SCHEDULE N/A since Unclassified	
4 PERFORMING ORGANIZATION REPORT NUMBER(S) MRC/WDC-R-110	5 MONITORING ORGANIZATION REPORT NUMBER(S) DNA-TR-87-41
6a NAME OF PERFORMING ORGANIZATION Mission Research Corporation 6b OFFICE SYMBOL (If applicable)	7a NAME OF MONITORING ORGANIZATION Director Defense Nuclear Agency
6c ADDRESS (City, State, and ZIP Code) 5503 Cherokee Avenue, Suite 201 Alexandria, VA 22312	7b ADDRESS (City, State, and ZIP Code) Washington, DC 20305-1000
8a NAME OF FUNDING/SPONSORING ORGANIZATION 8b OFFICE SYMBOL (If applicable) RAEV/Filios	9 PROCUREMENT INSTRUMENT IDENTIFICATION NUMBER DNA 001-85-C-0058
8c ADDRESS (City, State, and ZIP Code)	10 SOURCE OF FUNDING NUMBERS PROGRAM ELEMENT NO: 62715H; PROJECT NO: RX; TASK NO: RF; WORK UNIT ACCESSION NO: DH230790

11 TITLE (Include Security Classification)

HIGH-POWER MICROWAVE SOURCE CROSS-CALIBRATION/DIAGNOSTICS

12 PERSONAL AUTHOR(S)
Bollen, W. Michael and Bulson, Jeffry M.

13a TYPE OF REPORT	13b TIME COVERED	14 DATE OF REPORT (Year Month Day)	15 PAGE COUNT
Technical	FROM 841105 TO 850901	860204	80

16 SUPPLEMENTARY NOTATION
This work was sponsored by the Defense Nuclear Agency under RDT&E RMC Code B3460764662 RX RF 00002 25904D.

17 COSATI CODES			18 SUBJECT TERMS (Continue on reverse if necessary and identify by block number)
FIELD	GROUP	SUB-GROUP	High-Power Microwaves Microwave Diagnostics High-Power Microwave Source Cross-Calibration
20	14		
14	2		

19 ABSTRACT (Continue on reverse if necessary and identify by block number)

A high-power microwave (HPM) cross-calibration diagnostic package has been designed, constructed, and fielded on the DNA HPM source, Vircator I, at Physics International Company. The diagnostic was designed to measure HPM energy, peak power, pulse shape, frequency, and mode. The energy is measured with a calorimetric load, the peak power and pulse shape are measured with a homodyne detector with 350 ps rise-time response, time-resolved frequency is measured with a heterodyne detector, and mode measurements are obtained with a leaky-pipe radiator. The source operated and was diagnosed in the 8-12 GHz frequency range. Representative results are presented for 64 cross-calibration shots.

20 DISTRIBUTION/AVAILABILITY OF ABSTRACT	21 ABSTRACT SECURITY CLASSIFICATION
☐ UNCLASSIFIED/UNLIMITED ☒ SAME AS RPT ☐ DTIC USERS	UNCLASSIFIED
22a NAME OF RESPONSIBLE INDIVIDUAL Sandra E. Young	22b TELEPHONE (Include Area Code) (202)325-7042 / 22c OFFICE SYMBOL DNA/CSTI

DD FORM 1473, 84 MAR 83 APR edition may be used until exhausted
All other editions are obsolete

SECURITY CLASSIFICATION OF THIS PAGE
UNCLASSIFIED

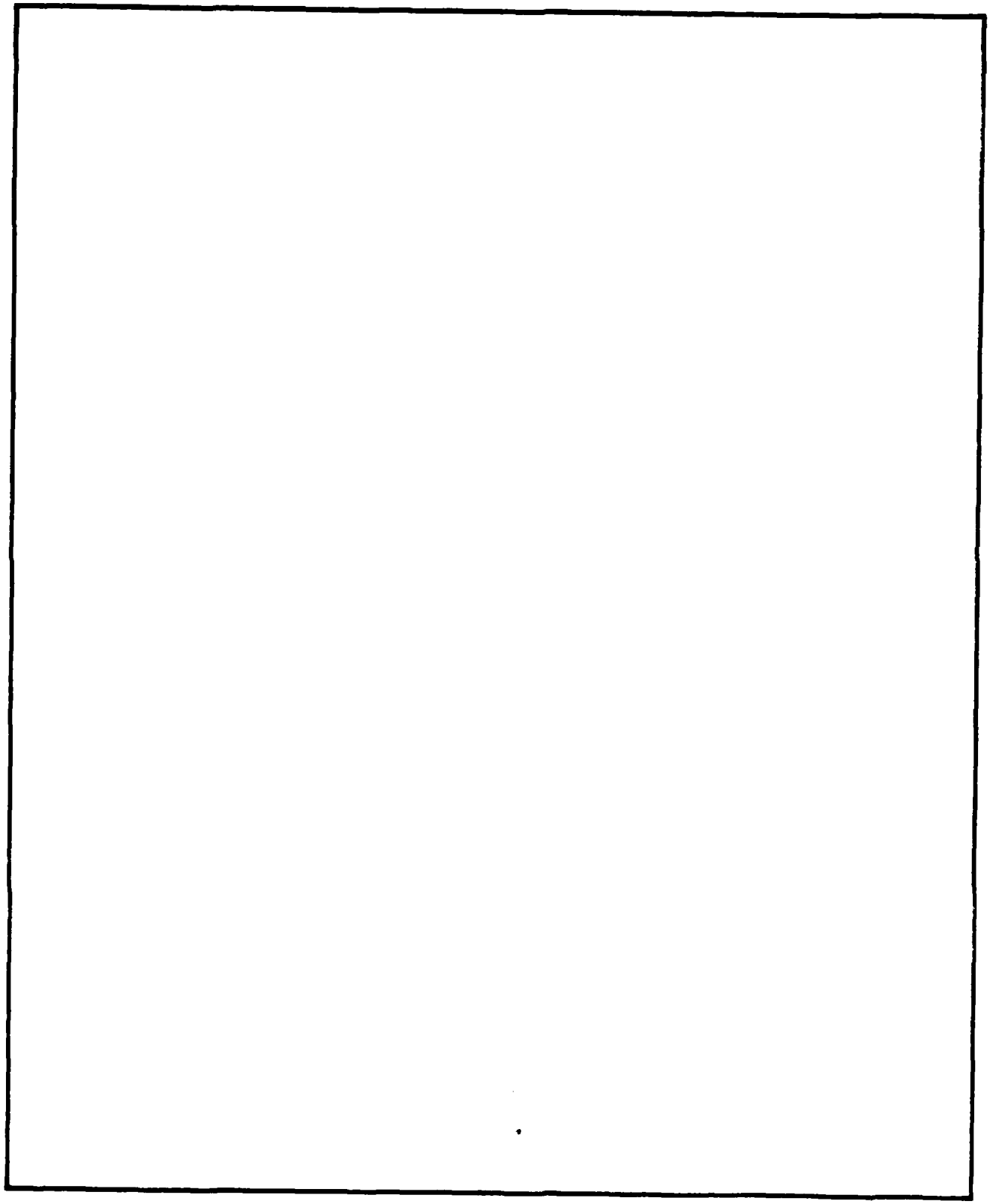

TABLE OF CONTENTS

LIST OF FIGURES

LIST OF FIGURES (continued)

LIST OF FIGURES (continued)

SECTION 1
INTRODUCTION

Over the past several years, the Defense Nuclear Agency (DNA) has been pursuing a program to assess the vulnerability of various military systems to high-power microwaves (HPM). In order to perform this work, DNA has established and assisted in establishing several HPM facilities (e.g. Physics International (PI), Sandia National Laboratories (SNL), and the Air Force Weapons Laboratory (AFWL)). During the past year, Mission Research Corporation (MRC) has been performing contract work for DNA to cross-calibrate these facilities. The purpose of this work has been to develop a cross-calibration diagnostic package and to begin calibrating the facilities. The cross-calibration will serve two purposes: 1) to allow data taken at different facilities to be compared in a systematic way, and 2) to provide an impartial check on the facility diagnostics. To date, only the PI side-extraction vircator has been calibrated.

The basic cross-calibration diagnostic package has been designed to measure HPM energy, peak power, pulse shape, frequency, and mode. These characteristics depend primarily on the HPM source. It is planned to extend the diagnostic package to include far-field mapping of the HPM field pattern. Energy information is obtained using a calorimetric load which utilizes an inverted cone design. This design has been shown to be sensitive to about 0.2 joules which is more than is required for the planned applications. Peak power is obtained from pulse-shape diagnostics. Using the measured energy and the pulse shape, the peak power can be calculated, since energy per unit time is related to power. Additionally, knowing the calibration of the pulse-shape diagnostic, a peak power may be measured directly. The latter approach is more susceptible to error than the former approach due to the large attenuation used in the pulse-shape diagnostic, but serves as a check on the other approach. The device utilized to measure the pulse shape is a double balanced mixer with a fast (4 GHz) IF output (Reference 1) yielding a 350 ps rise time using a TEK 7104 (1 GHz) oscilloscope. A heterodyne mixer

technique is utilized to measure the frequency (Reference 1). This approach down-converts the microwave signal to a frequency that can be directly measured on a fast (TEK 7104) oscilloscope. Mode is determined by using a leaky-pipe technique. This approach basically disperses the microwave pulse to different angles depending on the mode. Multiple pulse-shape detectors are then used to compare the energy in different modes. These diagnostic techniques are described in more detail in Section 2.

This diagnostic package has been utilized to calibrate the PI side-extraction vircator and worked extremely well. A schematic of this diagnostic package is shown in Figure 1. Energy per pulse was measured to be 7 ± 2 joules. Peak power was measured to be approximately 1.2 GW. The pulse shape was observed to consist of a few, very sharp (rise time of less than 0.5 ns), very narrow (FWHM = 1-2 ns) spikes. (This was the first time this structure was observed on the PI facility due to the slower diagnostics (rise time = 6 ns) that had been utilized.) The frequency was observed to chirp in time and to vary as expected when the AK gap of the vircator was varied. The mode content was measured to be 89% TE_{01}, 4% TE_{02}, and 7% TE_{03}. A detailed description of the data obtained for the PI cross-calibration is given in Section 3.

Based on our experience over the last several years during which MRC has performed HPM diagnostic work for DNA, MRC has identified four diagnostic technical areas that require additional work to assure a high quality HPM program for DNA: 1) improved diagnostic documentation as well as the availability of expert technical advice for the DNA HPM program, 2) refinements to the existing diagnostic package, 3) cross-calibration of other DNA facilities, and 4) the development of new diagnostics for lethality testing and for HPM propagation studies.

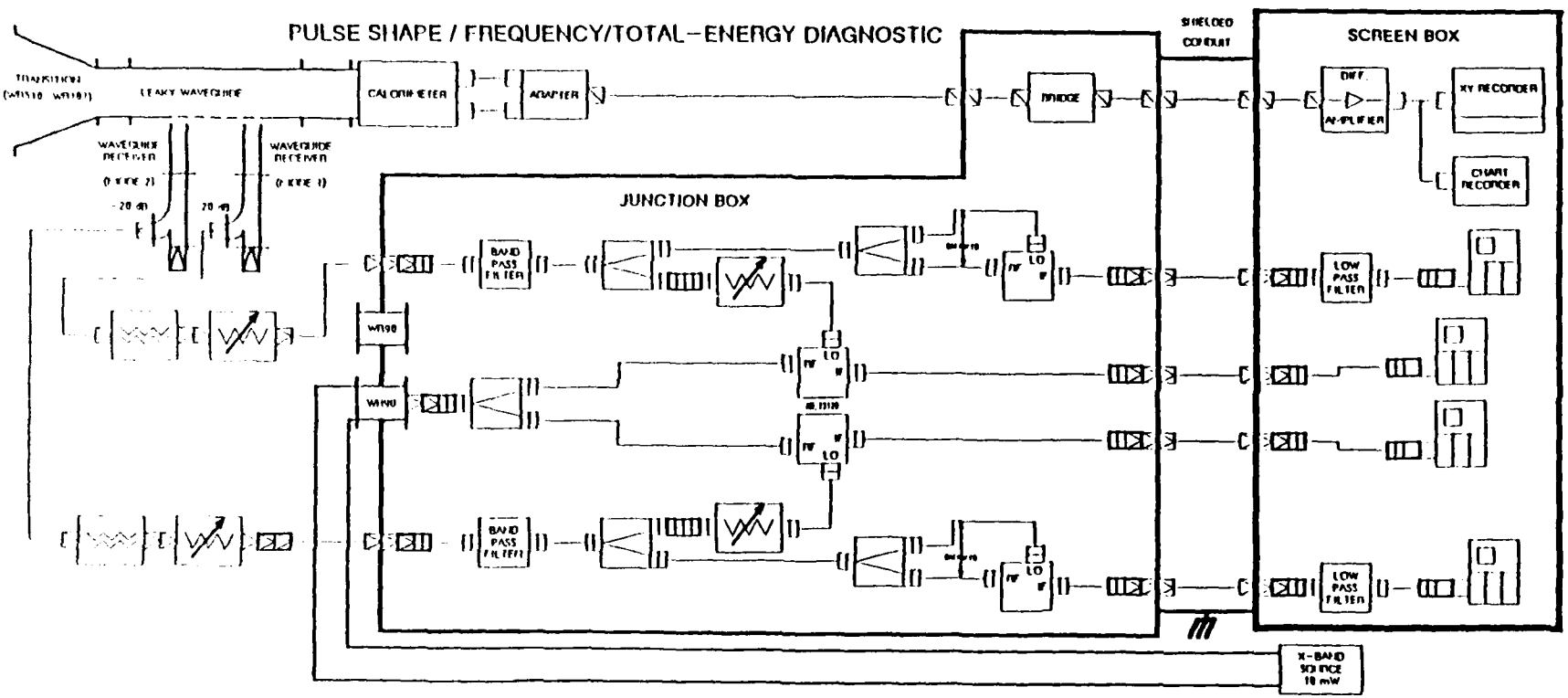

Figure 1. Schematic of cross-calibration diagnostic package.

SECTION 2
HPM DIAGNOSTICS

The purpose of this section is to describe in detail the diagnostic techniques utilized in our cross-calibration package. These techniques are 1) mixer pulse shape detector (homodyne), 2) mixer frequency detector (heterodyne), 3) calorimetry, and 4) leaky-pipe mode spectrometry.

2.1 HYBRID DOUBLE-BALANCED MIXER DETECTOR.

2.1.1 Introduction.

It is possible to use the diodes in mixers, with their inherent wide bandwidth, to detect the pulse shape/power of a microwave pulse. The essence of the technique is as follows. The high-power signal is attenuated to under 10W peak by waveguide side-wall couplers and fed coaxially into an in-phase, 2-way multi-octave Wilkinson power divider where it is coherently split. These two signals are fed via a matched coaxial pair into the RF and LO inputs of a hybrid double-balanced mixer with an IF bandwidth of 4 GHz. (Mixers are discussed in great detail in Section 2.2.) Since the frequencies are identical, the IF output is the pulse envelope with rise time resolution of about 70 ps. This signal is then measured by a fast oscilloscope (3 dB down at 1 GHz). This method is compact, simple to use, and cost competitive with crystal detectors. The frequency response has the potential to be essentially flat over its bandwidth, which is better than an octave in magnitude. Insertion loss and voltage standing wave ratio (VSWR) are low, and both components are available commercially for frequencies up to 18 GHz.

2.1.2 Physics.

The two major components necessary to construct this diagnostic are a power divider and mixer. Mixers are discussed in detail in Section 2.2 although comments regarding specific mixer attributes for a pulse shape diagnostic will be given here.

The mixer falls into the solid-state class of components, along with diodes, amplifiers, etc. The power divider falls into the passive component class, along with terminations, attenuators, shorts, directional couplers, etc. Because the power divider belongs to this class, it possesses the capability of withstanding high power (compared with solid-state devices) and is less susceptible to physical damage. Power dividers simply split an input signal into two or more identical output signals, or combine multiple signals into one output signal. The basic measure of quality of a power divider is its ability to provide identical outputs. However, achievement of equal outputs is also a function of the impedance match between the divider and the external system and of the intrinsic isolation of the divider.

There are several parameters which are useful when characterizing the performance of a power divider. The VSWR is a standard measurement for most microwave devices and is defined in Section 2.2. For multi-port systems, like the power-divider, VSWR measurements are made on a single port with the others terminated with matched loads. VSWR for power dividers is usually between 1.0 and 2.5.

The term isolation is defined as the ratio of the output power of one output port to the input power of any other output port and is expressed in dB. It is a measure of the isolation between any set of output ports. The measurement is made with matched terminations on all other ports. Isolation is typically between 10 and 20 dB for most dividers.

The insertion loss is a measure of the power loss through the device (excluding the power division factor). It is defined as the ratio of power output to power input and is expressed in dB. A matched source and load is used in the measurement. Since transmission line loss increases with frequency, the insertion loss is minimized at the lowest frequency and linearly increases with a slope dependent on the divider length. Insertion loss can be as low as .25 dB and may reach as high as 3 dB for multi-port dividers.

The amplitude tracking error is a measure of the difference in the signal amplitude at the output ports. It is sometimes called the amplitude unbalance. It is defined as the ratio of the maximum signal at any port to the minimum signal of any other port and is expressed in dB. Typically, the tracking error is very low, increasing with the number of output ports. It is usually under 1.0 dB.

The phase tracking error is a measure of the difference in phase of the signals measured at the output ports. It is defined as the maximum difference in the phases between the signals measured at any two output ports. It is typically very low and usually does not exceed ± 5° for most dividers.

2.1.3 Pulse Shape Detection.

There are several types of power dividers with unique attributes and problems. The unmatched coaxial type is simply economical. It cannot compete with other dividers on any other feature. The matched coaxial type boasts low VSWR and insertion loss, and high power capability as well as low cost. Its amplitude and phase tracking characteristics are poor, however. The Wilkinson stripline type has some of the best phase and amplitude tracking characteristics as well as the lowest insertion loss and high isolation. They are physically small and operate over a large bandwidth. The VSWR for this type divider is mediocre, however, and it has lower power handling capabilities. The tapered line stripline can handle more power than the Wilkinson stripline, but only at the expense of insertion loss and output tracking error. It does so, however, in a very large bandwidth. Finally, the characteristics of the microwave integrated circuit type are similar to those of the Wilkinson type, except that small size is exchanged for good insertion loss.

For pulse shape measurements using this technique, a mixer with the following characteristics is necesary: wide IF bandwidth, low VSWR (to enhance divider output tracking), high dynamic range, enhanced spurious

rejection and harmonic suppression, and substantial power handling capabilities. A detailed description of these parameters is given in Section 2.2.

The most critical consideration when choosing components for this diagnostic is to deliver to the mixer diodes two identical signals. This can be accomplished with a power divider with excellent amplitude and phase tracking characteristics and a mixer with well matched (balanced) LO/RF inputs. Based primarily on this consideration, the in-phase, two-way multi-octave Wilkinson stripline power divider used in conjunction with a 3 dB hybrid double-balanced mixer are the components of choice when constructing this diagnostic.

The schematic diagram shown in Figure 2 is that of a standard mixer detector. The specific components are described above. Construction of the matched coaxial pair requires great care, particularly for diagnostics at higher frequencies. Semi-rigid cable with gentle bends is recommended for enhanced performance. The use of identical phase shifters inserted in the matched coaxial pair line may improve performance. Once in the lines, they may be used to match exactly the phases of the two signals reaching the mixer diodes. Introduction of phase shifters may jeopardize the phase and amplitude tracking of the power divider, however, due to the additional VSWR.

Figure 3 is a typical example of double-balanced mixer detector data. The components were the following: Anaren 41690 power-divider: 7.0-18 GHz RF bandwidth, 20 dB isolation, 1.7 VSWR, 1.0 dB insertion loss, ± .25 dB amplitude tracking error, ± 5° phase tracking error, and Anaren 75129 double balanced mixer: 8.0-18 GHz RF bandwidth, 23 dB LO/RF isolation, 3.0 VSWR, 8.5 dB conversion loss, and DC-4.0 GHz IF bandwidth. The matched coaxial pair were 0.141" copper jacket semi-rigid cable with teflon dielectrics. The connectors used were beryllium copper SMA type straight connectors with the following characteristics (at 10 GHz): 1.1 VSWR, 0.09 dB insertion loss, 90 dB RF leakage. Figure 4 is the detected

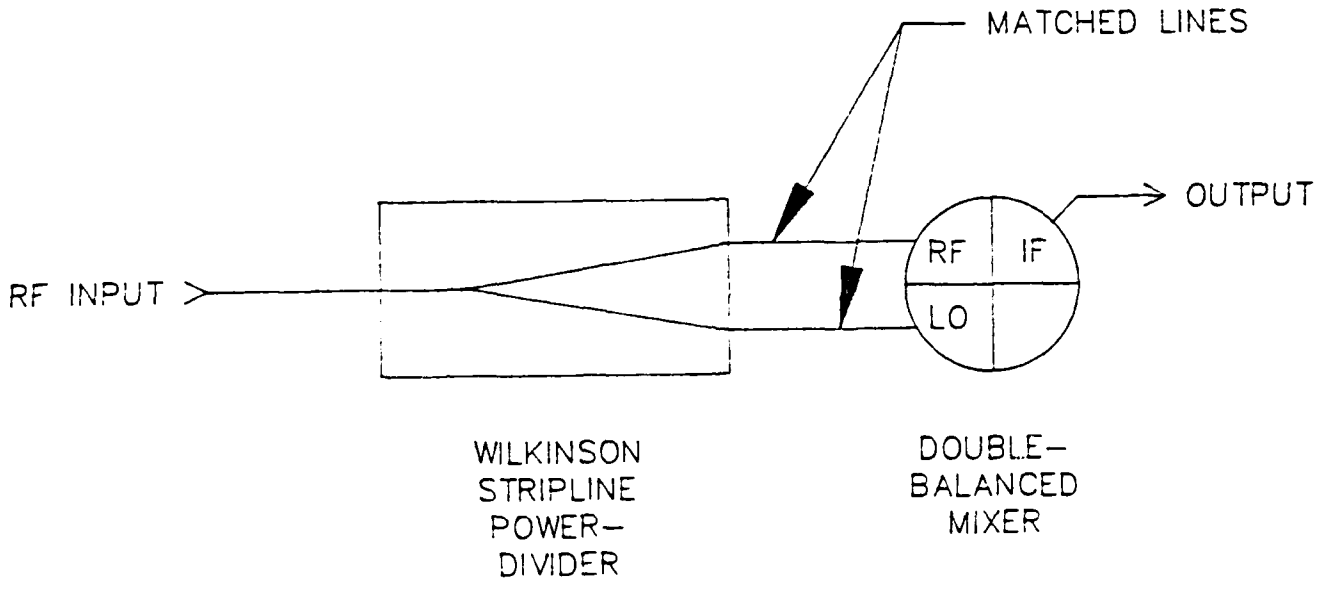

Figure 2. Double-balanced mixer detector.

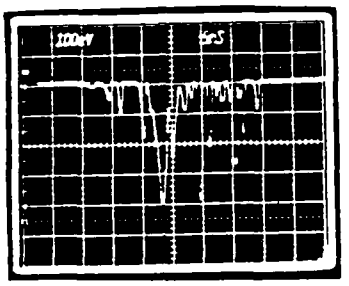

Figure 3. Double-balanced mixer pulse shape detector response.

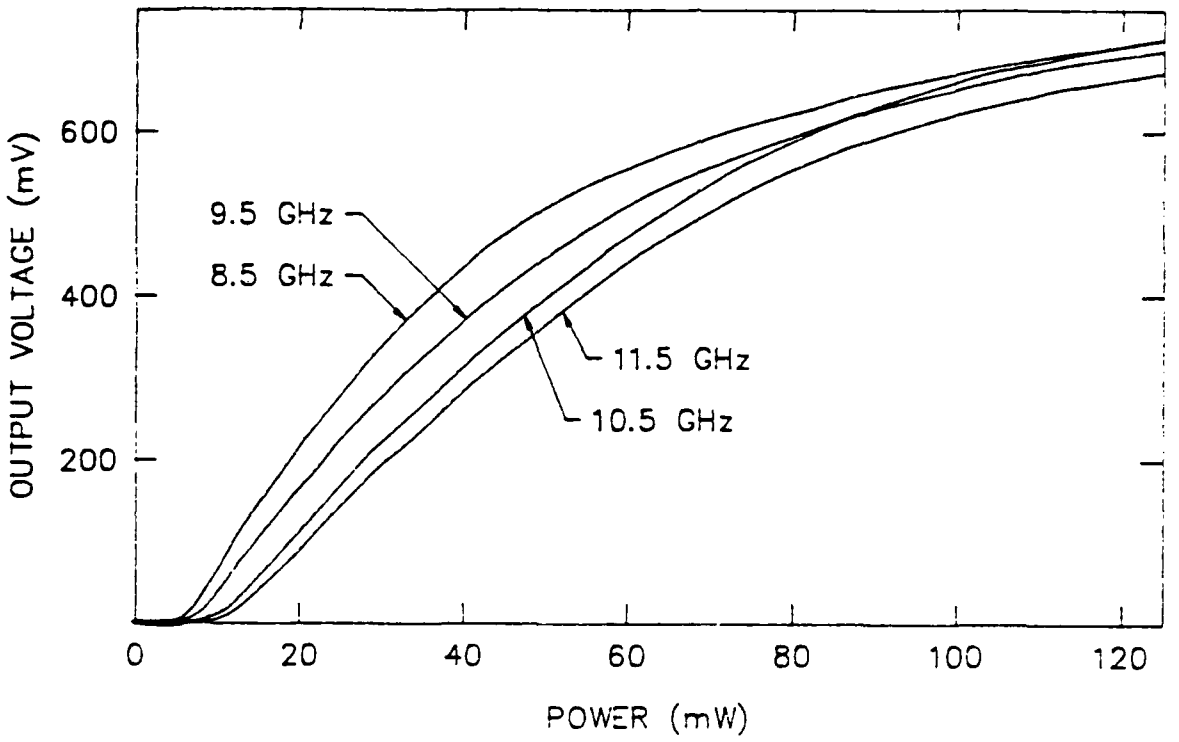

Figure 4. Calibration for double-balanced mixer detector.

RF power vs. output voltage curve for the above described detector. Curves are shown for four representative frequencies spanning the lower portion of the RF bandwidth of the mixer. The frequency response, although not flat, is similar to that of most crystal diodes. It is, however, a function of many factors, including VSWR throughout the system, phase tracking into both legs of the double-balanced mixer diode bridge, as well as the diode characteristics themselves. However, the use of the double-balanced mixer bridge should help average out unique frequency response effects of the diodes. Because the power-divider introduces an insertion loss of about -1 dB in addition to the power division factor of -3 dB, only about 40% of the input power is applied to each mixer port. The mixer described above will operate properly with an RF input of 400 mW: hence, signals in excess of 1W are detectable with no external attenuation. The rise-time characteristics, although qualitatively shown in Figure 3, have been measured for the mixer detector described above used in conjunction with a TEK 7104 scope with a 7A29 plug-in amplifier. This mixer detector rise-time response is shown in Figure 5. The 10%-90% rise-time for a 200 mV equivalent pulse is 300 ps which exceeds, by a factor of 2, the rise-times of the fastest Germanium Tunnel diodes (Reference 2).

Mixers are available with "RF" bandwidths from very low frequency (<1 Hz) to far into the sub-millimeter wave regime. Although not presently available commercially, mixers operating at 890 GHz with -25 dB rejection and about 1 dB insertion loss are being developed (Reference 3). Balanced and double-balanced mixers are readily available up to 110 GHz with RF bandwidths which span two octaves and IF bandwidths up to 8 GHz. Power dividers are available up to 220 GHz, although phase and amplitude tracking error become quite significant at frequencies above 20 GHz where stripline technology is no longer available. As mentioned above, this detector will operate in the 1-2 W maximum input range and will withstand twice as much power without damage, although the output may not be usable at this level. Although pulse shapes with 70 ps rise-times are detectable, state-of-the-art oscilloscopes limit the response to about 300 ps.

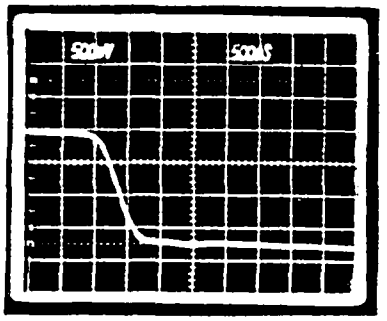

TEK 284 Gating Pulse

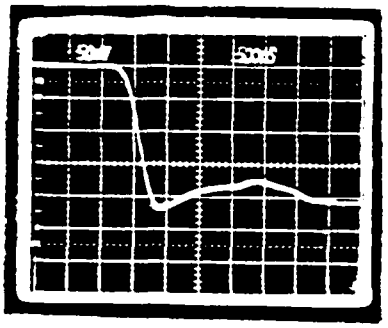

Mixer Detector Response

Figure 5. Rise-time response for mixer detector.

The advantages and limitations of using the "mixer" technique for microwave pulse shape measurements are summarized below.

Advantages

1) extremely fast rise-times (<70 ps without oscilloscope, <300 ps with TEK 7104/7A29)

2) simplicity of operation

3) multi-octave bandwidth

4) simple, straightforward design

5) moderate power handling capability (<2 W CW)

Limitations

1) wide unit-to-unit variation in characteristics

2) temperature and x-ray sensitivity

3) moderately expensive (approximately $1,000/channel)

2.2 MIXER HETERODYNE FREQUENCY DETECTOR.

2.2.1 Introduction.

Mixers are used to convert a signal from one frequency to another. This is done by combining the original RF signal with a local oscillator signal (LO) in a non-linear device such as a Schottky-barrier diode. The diode output spectrum has the following components: f_{RF}, f_{LO}, and $mf_{LO} \pm nf_{RF}$, where m and n are positive integers. The desired output frequency, commonly called the intermediate frequency (IF), can be either the lower ($f_{LO} - f_{RF}$) or the upper ($f_{LO} + f_{RF}$) sideband. When a mixer is used as a down-converter, the lower sideband is the sideband of interest. A balanced mixer makes use of the 3 dB hybrid to divide and recombine the RF and LO inputs in two mixing diodes in such a way as to distribute the signals uniformly (balanced) to each mixer diode. The necessity for a balanced mixer will be made clear in Section

2.2.2. The signal to be diagnosed is the RF input to the mixer, and the LO input is an appropriately selected, stable, local oscillator. The IF signal is then displayed on a wide-band oscilloscope as the down-converted RF signal shifted in frequency by exactly f_{LO}.

2.2.2 Physics.

The schematic diagram of a mixer is shown in Figure 6. The diode's nonlinear barrier resistance R_j performs the mixing while the other components (parasitics) merely introduce loss. In conventional resistive mixing, the nonlinear barrier resistance generates higher order harmonics of the local oscillator fundamental (f_{LO}), all of which mix with the input signal to produce the spectra described above. Third order harmonics and higher are not usually significant in most mixer designs; hence the following IF spectra includes all important components (listed from lowest to highest frequency): $f_{RF} - f_{LO}$, $2f_{RF} - 2f_{LO}$, f_{LO} (normally lower in frequency than f_{RF} but higher power), f_{RF}, $2f_{LO}$, and $2f_{RF}$.

There are two basic forms of the conventional mixer circuit. The simplest is the single-ended circuit which is comprised of a single diode and requires that the LO and RF be combined prior to their introduction into the mixer. The balanced mixer circuit consists of two diodes fed by a four-part, 3 dB coupler as shown in Figure 7. This configuration provides better isolation between the LO and RF signal and cancels the AM noise generated by the LO.

The theory of the mixing phenomenon is given in the following section. The I-V characteristic of a detector diode is given by

$$I_j = I_{sj}\left(e^{eV/n_jkT} - 1\right) , \qquad (1)$$

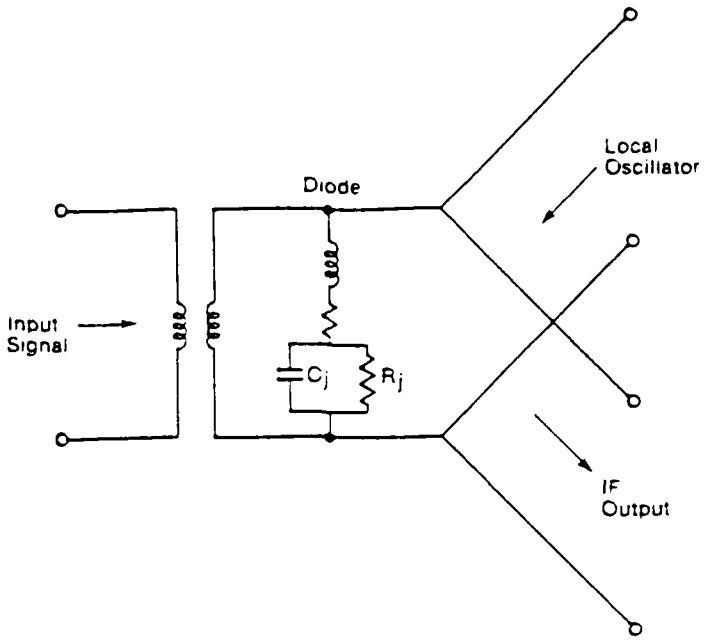

Figure 6. Schematic diagram of a mixer.

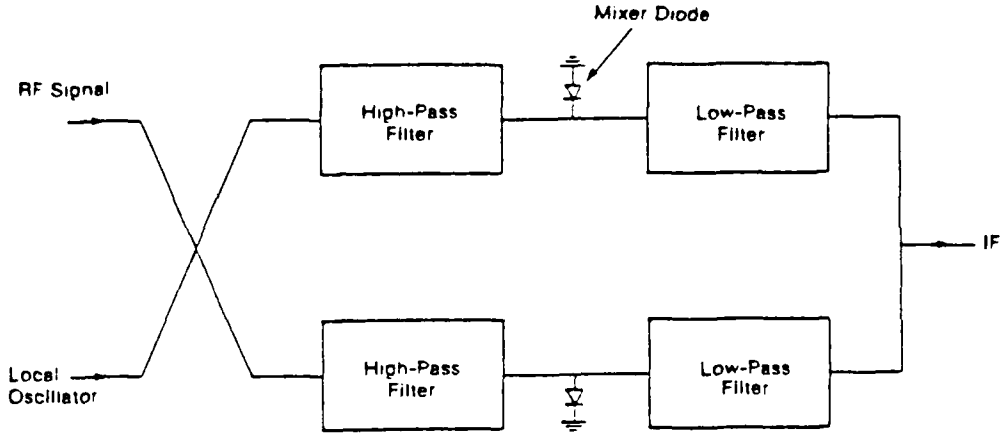

Figure 7. Basic balanced mixer configuration.

where I_{sj} = saturation current; k = Boltzmann's constant; e = electron charge; T = temperature; n_j = diode type factor .

p-n	Ge	j=1	n_j=1
	Si	2	≈2
Schottky	W-Si	3	≈1
	W-GaAs	4	≈1

Hence, the instantaneous conductance is given by

$$g(t) = \frac{\partial I_j}{\partial V} = \frac{eI_{sj}}{n_j kT} \exp\left(\frac{eV}{n_j kT}\right) \tag{2}$$

where

$$V = V_0 + V_{LO} \cos \omega_{LO} t \ . \tag{3}$$

(The LO voltage alone determines the conductance only if it is much larger than the RF voltage. If the reverse is true, the LO and RF subscripts are interchanged.) Expanding the exponential in terms of Bessel functions, the general form for g(t) may be written

$$g(t) = g_0 + \sum_{m=1}^{\infty} 2\, g_m \cos m\omega_{LO} t \tag{4}$$

where

$$g_m = \frac{eI_{sj}}{n_j kT} \exp\left(\frac{eV}{n_j kT}\right) I_m\left(\frac{eV_{LO}}{n_j kT}\right) \quad , \quad m=0,1,2,\ldots \tag{5}$$

with $I_m(x)$ denoting the modified Bessel functions. Hence, the predominant voltage across the nonlinear diode provides us with the conductance. Now, when an RF signal is applied, the total voltage across the diode is given by

$$V_T = V_0 + V_{LO}\cos\omega_{LO} t + V_{RF}\cos\omega_{RF} t \ . \tag{6}$$

Substituting V_T in (1) for V and expanding in a Taylor's series about V_0 + $V_{LO}\cos\omega_{LO}t$ (=V) for the current, we have

$$I_j(V_T) = (V_T - V)\frac{\partial I_j(V_T)}{\partial V_T} + O(V_T - V)^2$$

$$= g(t)V_{RF}\cos\omega_{RF}t + O(V^2_{RF}) \quad . \tag{7}$$

Substituting (4) in (7) for g(t) we have

$$I_j = g_0 V_{RF}\cos\omega_{RF}t + \sum_{m=1}^{\infty} g_m V_{RF}[\cos(m\omega_{LO} + \omega_{RF})t + \cos(m\omega_{LO} - \omega_{RF})t] \quad . \tag{8}$$

Hence, (8) provides an expression for the diode current spectra which appears at the IF port of the mixer. When used as a down-converter, suitable low-pass filters are utilized to transmit only those frequencies of interest (i.e., predominantly the $\cos(\omega_{LO} - \omega_{RF})t$ term).

A variety of parameters have been defined in order to characterize the performance of individual as well as each class of mixer circuit. Conversion loss (L_C) and noise figure (F_N) are two of the most important and closely related mixer parameters. Conversion loss is a measure of the efficiency with which a mixer converts the RF signal into an IF signal. It is defined as the ratio of RF power to IF power at fixed LO power and is expressed in dB. The noise figure is defined as the ratio of the IF power to available IF noise power and can be expressed in terms of the conversion loss as follows:

$$F_N = L_{RF}L_C N_R \tag{9}$$

where L_{RF} is the RF transmission loss of the input circuit and N_R is the ratio of the IF output power to the noise power of an impedance equal to that of the diode at the IF frequency when driven by the LO.

The VSWR is a measure of the impedance match between each of the mixer LO and RF ports and the 50 ohm system in which it is used. It can be expressed in terms of the reflection coefficient of that port as follows:

$$r = \frac{1 + \sqrt{R}}{1 - \sqrt{R}} \quad . \tag{10}$$

This reflection coefficient is, in turn, dependent on the diode reflection coefficients for each hybrid configuration. Reflections from the similar mixing diodes in a 90° hybrid mixer will combine at the input opposite to the one being fed, resulting in low VSWR at either port. As shown in Equation (11) for the input reflection coefficient of a 90° hybrid, balanced diodes will result in a matched input, whatever their value,

$$R_{90° \text{ hybrid}} = \frac{1}{2} (R_1 - R_2) \quad . \tag{11}$$

Here R_1 and R_2 are the reflection coefficients for each diode. The 180° hybrid, on the other hand, focuses any reflections from the similar mixer diodes back to the input port. Unless the diodes themselves are a very good match, the VSWR will be very poor. The expression for the input reflection coefficient for the 180° hybrid is given by Equation (12),

$$R_{180° \text{ hybrid}} = \frac{1}{2} (R_1 + R_2) \quad . \tag{12}$$

If the diode impedances are equal, the input VSWR is the return loss for just one diode. As demonstrated in Equation (2), diode impedance (and hence 180° hybrid VSWR) is a function of LO drive power (if the LO power dominates over the RF power). (Note: The quad fed dual and double balanced mixers shown in Table 1 use 90° hybrids and 180° hybrids, respectively, as the coupling networks to their diodes and hence exhibit VSWR characteristics similar to their simpler counterparts.)

The LO/RF isolation is a measure of the LO power leakage to the RF port of the mixer. It is defined as the difference between the LO power levels at the LO port and the RF port and is expressed in dB. Here, 180° hybrid types enjoy the best performance. The isolation for 180° hybrids is given by

Table 1. Comparison of Each Class of Mixer with Representative Values for Each Performance Parameter.

Type	#Diodes	VSWR	L_c(dB)	LO/RF Isolation	Spurious Rejection	Harmonic Suppression	IF Bandwidth
Balanced 90° Hybrid	2	1.3	5-7	10	poor	poor	wide
Balanced 180° Hybrid	2	2.5	7-9	20	fair	good	wide
Balanced Quad Fed Dual	4	1.3	7-9	30	good	fair	wide
Double Balanced	4	2.5	7-9	40	good	very good	extremely wide

$$\text{Isol.}_{180°} = 20 \log \left(\frac{2}{R_1 - R_2} \right) \tag{13}$$

and hence is strongly enhanced for matched diodes. One must note, however, that the diodes must track each other with LO input power to retain these enhanced characteristics. The 90° hybrid types do not fare as well, however, since any LO power not absorbed by the diodes is directed to the RF port. The isolation for this type of coupling network is given by

$$\text{Isol.}_{90°} = 20 \log \left(\frac{2}{R_2 + R_2} \right) . \tag{14}$$

For matched diodes, the isolation will be the return loss for one diode. (Note: The double-balanced mixer uses 180° hybrids as the coupling network and hence enjoys the same characteristics as the balanced 180° hybrid mixers. Although quad fed mixers use 90° hybrid coupling networks, their LO/RF isolation performance is also good due to a phasing network designed to dump unused LO power into an internal load.)

The desired IF output of a mixer used as a down-convertor is the lower sideband (LSB): $f_{IF} = f_{RF} - f_{LO}$. As mentioned above, the LSB is hardly the only component present at the IF port, and it is frequently a design consideration to suppress all other signals. There are several parameters to describe each class of unwanted harmonic or spurious response. In order to classify these harmonics, a system has been defined as follows. Harmonics are expressed in the form $mf_{LO} + nf_{RF}$ and are classified by their order: (m+n)th order or mxn. Roughly speaking, spurious rejection is a measure of how well the mixer prevents $|m-n|=1$ spurious responses from reaching the IF port. Similarly, harmonic suppression is a measure of the mixer's ability to eliminate $|m-n|=0$, $m,n>1$ signals. Typically, signals with $m,n \geq 5$ or $|m-n| \geq 2$ are insignificant and hence are not discussed here. Both terms described above fall into

the category known as single-tone intermodulation due to the monochromatic nature of the RF and LO input signals. A representative graph of 90° hybrid mixer single-tone intermodulation response for $f_{RF}<100$ MHz is shown in Figure 8. Suppression of harmonic intermodulation products is dependent on the RF and LO phase and the diode junctions. Mixers are typically designed to suppress completely all even mxn harmonics. As shown in Figure 8, the only significant (within 30 dB) IF signals are the 1x1 and 2x1, and the 2x1 is 15 dB down from the LSB. Two-tone intermodulation is the result of two signals being applied to the mixer RF input simultaneously. They may generate harmonics, mix with each other, and mix with the LO and its harmonics. This produces a rather large spectrum of which the third-order, two-tone products are prevalent due to their magnitude and hardiness. The third-order products are $(2f_{RF1} \pm f_{RF2}) \pm f_{LO} = f_{IF}$ or $(f_{RF1} \pm 2f_{RF2}) \pm f_{LO} = f_{IF}$, and they follow a power law response similar to the single-tone response shown in Figure 8. A standard method of specifying the third-order performance is the "intercept" approach. The third-order intercept is the point at which the third-order response with a slope of 3 intercepts the "linearly" extrapolated 1x1 response with a slope of 1. Because the slope for a third-order response is always 3, the higher the intercept point, the better the suppression.

The IF bandwidth is typically defined as the upper and lower frequencies at which the IF response is at most 3 dB below the IF response at 30 MHz. Mixers are available with IF bandwidths as large as DC to 8 GHz in the millimeter wave range, and some IF bandwidths overlap the RF bandwidth. Large IF bandwidths are achieved with the application of phasing techniques to the IF ports rather than filtering to extract IF power.

The dynamic range is simply defined as the power range over which the device can be used. The following is a description of the regimes of interest for a mixer in order of increasing RF input power. Below the minimum detected signal (S_{min}) only thermal noise is present.

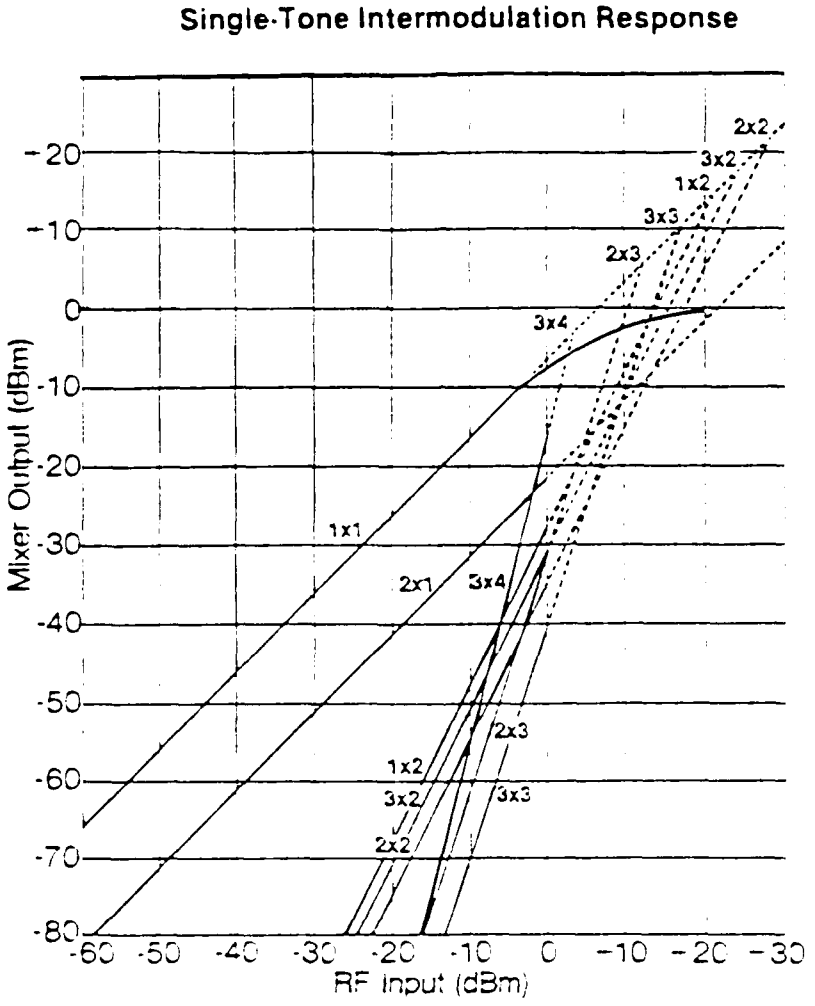

Figure 8. Single-tone intermodulation response.

An expression for S_{MD} is as follows:

$$S_{MD} = -111 \text{ dBm} + 10 \text{ dBm } \log(B_{IF}) \quad (15)$$

where the first term is 3 dB above thermal noise in a 1 MHz bandwidth and B_{IF} is the IF bandwidth normalized to 1 MHz. The spurious free dynamic range (R_{SF}) begins at S_{MD} and includes up to the maximum input level that generates third-order intermodulation products just equal to the output noise level. The dynamic range is typically identified as R_{SF} and can be written as follows:

$$R_{SF} = \frac{2}{3} [P_I - L_C - S_{MD}] \quad (16)$$

where P_I is the third-order intercept point normalized to 1 dBm and L_C is the conversion loss in dB. Here, S_{MD} is normalized to 1 dBm. The third-order intercept point is near the onset of mixer saturation which occupies the regime above R_{SF}. The mixer may still be useful in this regime if spurious rejection and suppression of two-tone intermodulation are unimportant. This is typically not the case with the mixer application of down-conversion. Finally, increased RF power will reach the damage level of the component which can exceed 1W CW.

2.2.3 Frequency Detection.

Several classes of mixer circuits have been developed. Each class of mixer circuit has a unique set of enhanced parameters to meet a specific need. Table 1 provides a comparison of each class with representative values for each parameter. The balanced mixer (180° hybrid type) is being replaced with the double-balanced mixer which enjoys equal or superior performance for all mixer parameters. All mixer types are suitable as down-converters and phase detectors. Only the double-balanced mixer is useful as an up-converter or for balanced or bi-phase demodulation purposes. On the other hand, the balanced mixers perform well as frequency discriminators and as AM or FM demodulators. Selection of a mixer with the proper characteristics is a necessity for hybrid mixer

down-converter frequency diagnostics. If the knowledge of the frequency to be measured is limited, an extremely wide IF bandwidth is required, although frequency measurement is bandwidth limited to about 1 GHz by present oscilloscope technology. Accurate, unambiguous frequency measurements always require a mixer which rejects m-n=1 spurious IF signals and severely suppresses harmonic generation. Conversion loss is usually not a concern because of the excess RF power available. According to Table 1, the double-balanced mixer has the best spurious rejection and harmonic suppression characteristics as well as an extremely wide IF bandwidth. The conversion loss is at an acceptable level, and the poor VSWR can be easily corrected with little or no detrimental effect on the performance of this frequency measurement tool.

The power of the double-balanced mixer down-converter is demonstrated in Figure 9a, where actual data is presented. The mixer was an Anaren 73129 double-balanced mixer with the following characteristics: 8.0-18 GHz RF bandwidth, 23 dB LO/RF isolation, 3.0 VSWR, 8.5 dB conversion loss, and DC-4.0 GHz IF bandwidth. The LO was driven at 8.5 GHz (30 mW). The IF output was measured in a 50 ohm system with a fast oscilloscope (3 dB down at 1 GHz). Despite the spikey nature of the pulse shape itself (Figure 9b), the frequency measurement responds satisfactorily because the high LO power drove the mixer into its flat, nonlinear regime, and the pulse shape was "washed out". The Fourier transform of Figure 9a is shown in Figure 10. Clear components are present at (8.5 ± 0.32) GHz and (8.5 ± 0.15) GHz. The inherent difficulty with this mixer technique is the ambiguity in the frequency measurement. Either an RF frequency higher or lower than the LO frequency will result in the same IF output. Hence, two diagnostics or two separate samples with different LO frequency are necessary to measure uniquely the frequency.

An area of concern and uncertainty with this technique (which is sometimes called the heterodyne technique) is in the difficulty of interpreting the results if the pulse width is near the period of the IF

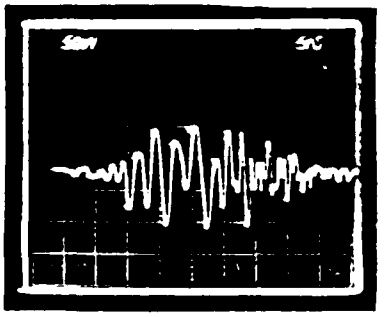

Figure 9a. Down-converted high-power microwave signal.

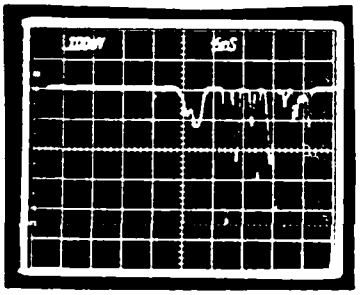

Figure 9b. Pulse shape of high-power microwave signal.

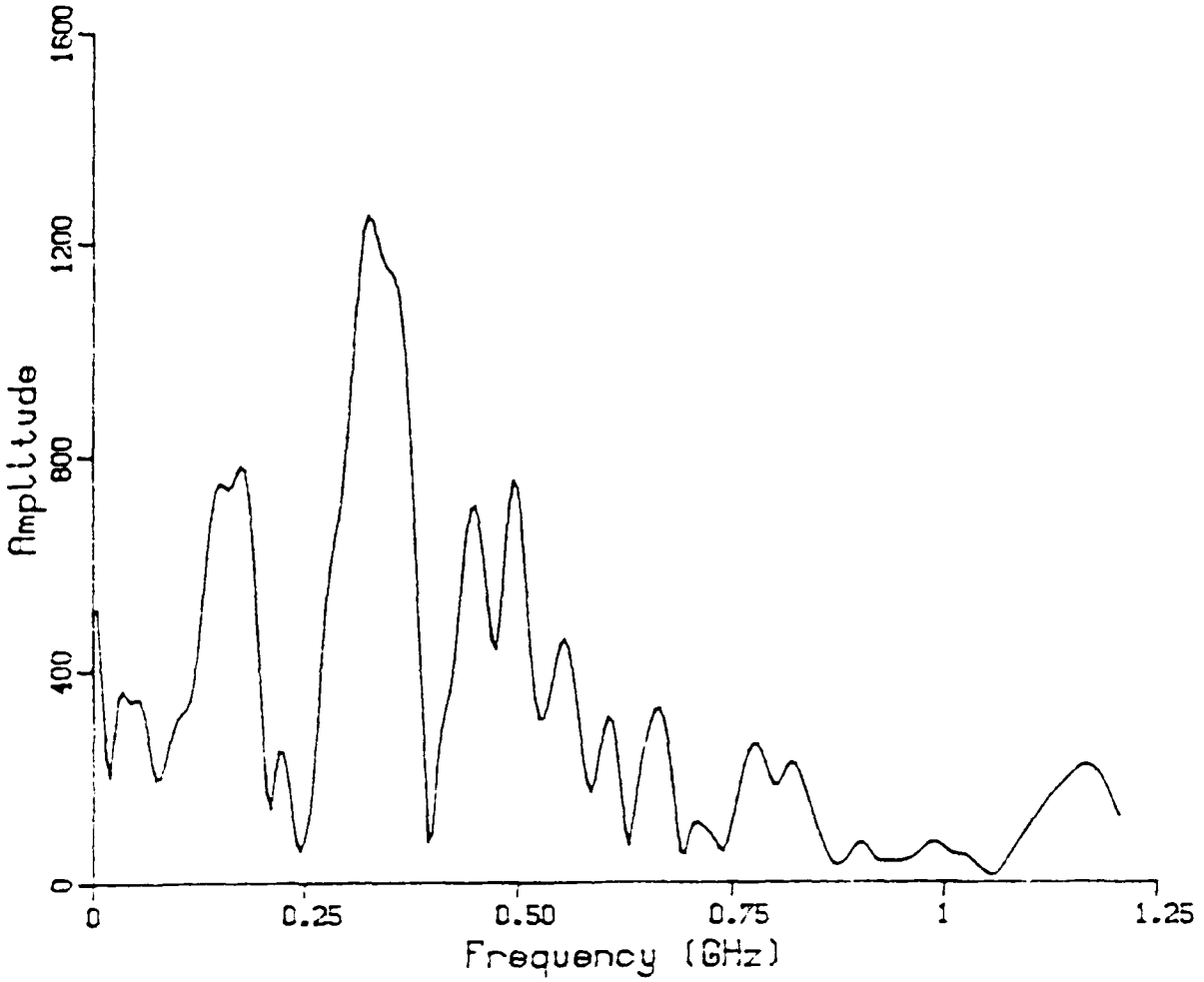

Figure 10. Fourier transform of signal shown in Figure 9a.

signal, $\tau_{pw} \leq (2f_{IF})^{-1}$. A full cycle or more of the down-converted signal is not observable in the output of the mixer, and the pulse shape cannot be extracted easily from the IF signal. Thus, the scope bandwidth limits the minimum pulse width for which a frequency measurement may be made. For example, if the scope bandwidth is 1 GHz, the pulse width limit is about 10 ns since about 10 cycles are desired to define the frequency. Also, this implies a limit on how quickly a signal can chirp inside the pulse. This condition must be investigated to gain insight into the interpretation of heterodyne results for short microwave pulses.

Mixers are available with RF bandwidths from very low frequency (<1 Hz) to far into the sub-millimeter wave regime. As mentioned above, mixers operating at 890 GHz are being developed and balanced mixers are readily available up to 110 GHz. Some RF bandwidths for individual units span several octaves, and IF bandwidths cover DC-4 GHz for some. Power handling capabilities do not exceed 1 W (usually < 400 mW).

The advantages and limitations of using the heterodyne technique as a microwave frequency diagnostic are summarized below.

Advantages

1) single-pulse frequency determination
2) easy to implement and use
3) usually simple to interpret output
4) time-resolved frequency measurement
5) instantaneous RF bandwidth spans several octaves
6) diagnostic less LO source is inexpensive
7) compact when VCO used as LO source
8) accurate frequency determination

Limitations

1) requires fast oscilloscope for measurement

2) frequency uncertainty must be less than 1 GHz

3) two diagnostics necessary for unambiguous measurement

4) oscilloscope bandwidth limits the minimum pulse width and/or the frequency chirping speed detectable with this method

5) input attenuation necessary to prevent detector damage

2.3 CALORIMETER.

2.3.1 Introduction.

Calorimetry is the fundamental microwave energy (average power) diagnostic technique. A calorimeter consists simply of a thermally isolated radiation absorber and a temperature transducer. An ideal absorber converts 100% of the incident electromagnetic radiation into thermal energy; conversion in this case is represented by the temperature rise of the absorber. The total energy of an incident microwave pulse can be calculated from the temperature rise of the absorber. The average power is calculated from a simultaneous measurement of the pulse shape.

Calorimeters are inherently broadband devices, i.e., over a wide frequency range the energy absorbed and the temperature rise of the absorber are not dependent on the incident frequency. Microwave calorimeters have been constructed and used in the S-, X-, and W-band ranges to diagnose short (< 30 ns), high power (~ 1 Gigwatt), non-repetitive pulses. The total pulse energy, however, may be less than one joule. This places a premium on the ability to detect small temperature changes.

2.3.2 Physics.

In theory and in practice, calorimeters are fairly simple devices, although careful engineering is required to maximize their performance. A calorimeter simply absorbs electromagnetic energy and converts it into thermal energy. The theory of operation is quite simple. If a thermally isolated body of mass M and specific heat C_p absorbs a quantity of energy Q, then the temperature of the body will increase by an amount, $\Delta T = Q/MC_p$.

There are two major areas that must be addressed: conversion of electromagnetic energy into thermal energy, and measurement of thermal energy change (usually via temperature). The former requires consideration of absorber material, geometry, and orientation as they relate to the conversion efficiency of electromagnetic to thermal energy, thermal losses, electromagnetic reflectivity (impedance matching), and frequency response. Other concerns include calorimeter sensitivity and response rise-times.

The equation above, relating temperature change to absorbed energy, is valid only for an ideally thermally-isolated absorber in thermal equilibrium. This ideal can be very closely approached in practice by minimizing thermal losses. In general, the three processes by which thermal energy may be lost in the system are radiation, conduction, and convection, in order of importance. Convective losses are all but eliminated by performing the calorimetric measurement in-vacuo. Conductive losses are minimized by utilizing thin monofilament support members with low thermal conductivity for the absorber material, and thin thermal transducer leads. For a calorimeter of mass M and specific heat C_p suspended with monofilament of cross-section A_0, total length ℓ_0, and thermal conductivity κ_0, the conductive thermal loss goes as a decaying exponential with e-folding time of $t_c = C_p M \ell_0 / \kappa_0 A_0$. For most calorimeters designed with bulk sheet absorber, the primary source of

thermal energy transport is radiative. Radiative losses are minimized with low absorber surface area and small temperature gradients between the absorber and the vacuum chamber. Recent developments have indicated that more stable calorimetric behavior is attained with an insulated vacuum chamber at room temperature rather than with ice baths. An explanation for this observation involves a variety of factors. Fluctuations in vacuum vessel temperature resulting from melting ice and variations in vessel pressure coupled with the large temperature gradient between vessel walls and input waveguide are the predominant temperature stability factors. Still, the radiative losses predominate, and energy is lost linearly in time with one-half of the absorbed energy lost after

$$t_{1/2} = \frac{C_p M \, \ell n(2)}{4\sigma A T_R^3} \qquad (17)$$

where σ = Boltzmann constant, A = calorimeter surface area, and T_R = reservoir temperature. Of course, these loss rates are meaningful only with reference to the rate at which the absorber reaches thermal equilibrium. For a conical shaped absorber of length ℓ made of material with specific heat C_p, thermal conductivity κ, and mass density ρ, thermal equilibration goes as a decaying exponential with an e-folding time of $t_{01} = (C_p \rho \ell^2)/(\kappa \alpha^2)$, where $\alpha = 4.5$. To demonstrate the relative magnitudes of the time constants listed above, take the example of a 15 cm long poco-graphite pyramid with a base dimension of 5.3 cm and thickness of 0.005". Assume it is suspended by nylon monofilament in 8 places and two thin copper wires connect the thermistors to the outside world. The e-folding time for conductive losses for the monofilament and the copper wires are 31 days and $1^1/_2$ hours, respectively. The radiative half-life is 23.6 s and the thermal equilibration rate is 15.3 s. This specific example will be discussed later in more detail.

There are a variety of materials available as electromagnetic radiation absorbers in the microwave regime. Most calorimeters for short

microwave pulses have utilized resistive absorbers. Since the absorber temperature is usually monitored in only a few locations, it is necessary that any absorber material possess a high thermal conductivity so that thermal equilibrium may be reached before the various heat loss mechanisms significantly reduce the absorber temperature. Poco-graphite is by far the most widely used material because of its low mass density, good absorption coefficient, and availability in thin sheets. Synthane-Taylor L-564 has a better absorption coefficient but is not available in sheets under 0.015" thick and has a mass density comparable to poco-graphite. Both materials are fairly rigid, preventing the construction of arbitrary shapes. Arbitrary shapes may be special ordered from Synthane-Taylor, however. Thin films of graphite are available on mylar films which allow flexibility in construction. The absorptive properties of this material, however, have not been investigated. Finally, research is being conducted on a resistive wire microwave absorber (Reference 4). This type of calorimeter requires no external transducer, since its resistivity is a function of temperature.

In order for the observed absorber temperature rise to represent truly the total pulse energy, either all of the incident energy must be absorbed, the fraction of energy absorbed must be frequency independent, or the frequency content of the pulse and the frequency response of the absorber must be known. The latter is less desirable and difficult to know accurately. In an engineering sense, this means that the absorber should be well matched to the source waveguide. This matching is accomplished in several existing designs that utilize pyramidal resistive absorber with taper lengths on the order of 5-10 wavelengths. However, other geometrical configurations have been used. Absorption coefficients are usually .90 or better. Several pyramid orientations are possible. Some designs place the pyramid apex closest to the source. A particular design in this configuration placed the apex near one wall of the waveguide in a region of low electric field strength to minimize electrical breakdown problems. This problem can be circumvented by placing the

pyramid apex away from the source. In any design, however, a compromise must be reached between two conflicting requirements: a long absorber is necessary for waveguide matching, and low absorber mass (mass proportional to length) is necessary for maximum sensitivity.

The method by which the temperature change is detected is discussed below. The average absorber temperature is typically monitored by several thermistors fastened to the absorber and electrically connected in series. Thermal contact is made through thermally conductive epoxy which afix the thermistors to the absorber. The absorber pieces themselves are usually adjoined with electrically conductive epoxy. The measurement sensitivity can be improved if the thermistor array is connected as one leg of an electrical resistance bridge circuit. Very small temperature changes, on the order of 1 mK, can be measured in this fashion. Care must be taken, however, to reduce possible thermistor ohmic heating effects. It has been suggested that an infrared camera, capable of measuring temperature changes of about .1°C, may be suitable as a calorimeter temperature transducer. This arrangement has two advantages: 1) any conduction losses through thermistor leads or thermistor self-heating effects are eliminated, 2) the temperature distribution of the entire absorber can be monitored, which can yield detailed information on the mode pattern of the incident radiation. A recent alternate approach differs in that the absorber temperature is not measured; instead, the thermal energy stored in the absorber is transferred to a gas cell bounded on one side by the absorber and on the other by an input window. The absorber is placed one-quarter wavelength in front of a conductive end plate. The incident energy is calculated from the measured pressure rise in the gas cell.

2.3.3 Calorimetric Energy Measurements.

The trend in HPM source development is toward lower frequencies in overmoded waveguide. This trend makes the application of calorimetric

techniques difficult, if not impossible. Physically large waveguide requires physically large calorimetric absorbers which suffer from poor sensitivity if properly impedance matched, or poor VSWR if the length is decreased to improve sensitivity. A careful design is necessary to insure performance characteristics consistent with the needs of the source being diagnosed. The performance characteristics of the calorimeter discussed in the third paragraph of this section are somewhat typical and will be presented below. The output of the HPM source to be diagnosed was overmoded C-band waveguide (1.5" x 3") at about 8 GHz with most of the power in the TE_{10} mode. VSWR measurements were taken in-situ (mounted in the vacuum chamber) and are presented in Figure 11. As is evident from the figure, the reflection coefficient varies radically over the band from under 1% to 76%. The calorimeter, however was designed for enhanced sensitivity which will be demonstrated shortly. The response itself was calculated based on the thermal equilibration and decay rates discussed above in addition to the inclusion of a resistance bridge circuit in the design. The sensitivity of 30 mV/J for this calorimeter is also dependent on the specific circuit component values used. Incorporating this sensitivity and the time constants calculated above, an estimate for the response can be made and is shown in Figure 12a. The actual response is shown in Figure 12b where the data has been corrected for VSWR. It should be noted that the response of some calorimeters resembles a step function, because the absorber surface area is small and radiative effects are essentially insignificant. For response of the type shown in Figure 12, the regime of interest is during the exponential decay which should be exponentially extrapolated to t = 0 to obtain the t = 0 response. Because flat frequency response was sacrificed for sensitivity, the calorimeter must be calibrated over the frequency band of interest. The frequency response for the above calorimeter is shown in Figure 13. Methods to improve frequency response while maintaining sensitivity and mode independency are being investigated. Finally, as expected, the response of the calorimeter with incident energy is linear. The response of the calorimeter discussed above as a function of incident energy is shown in

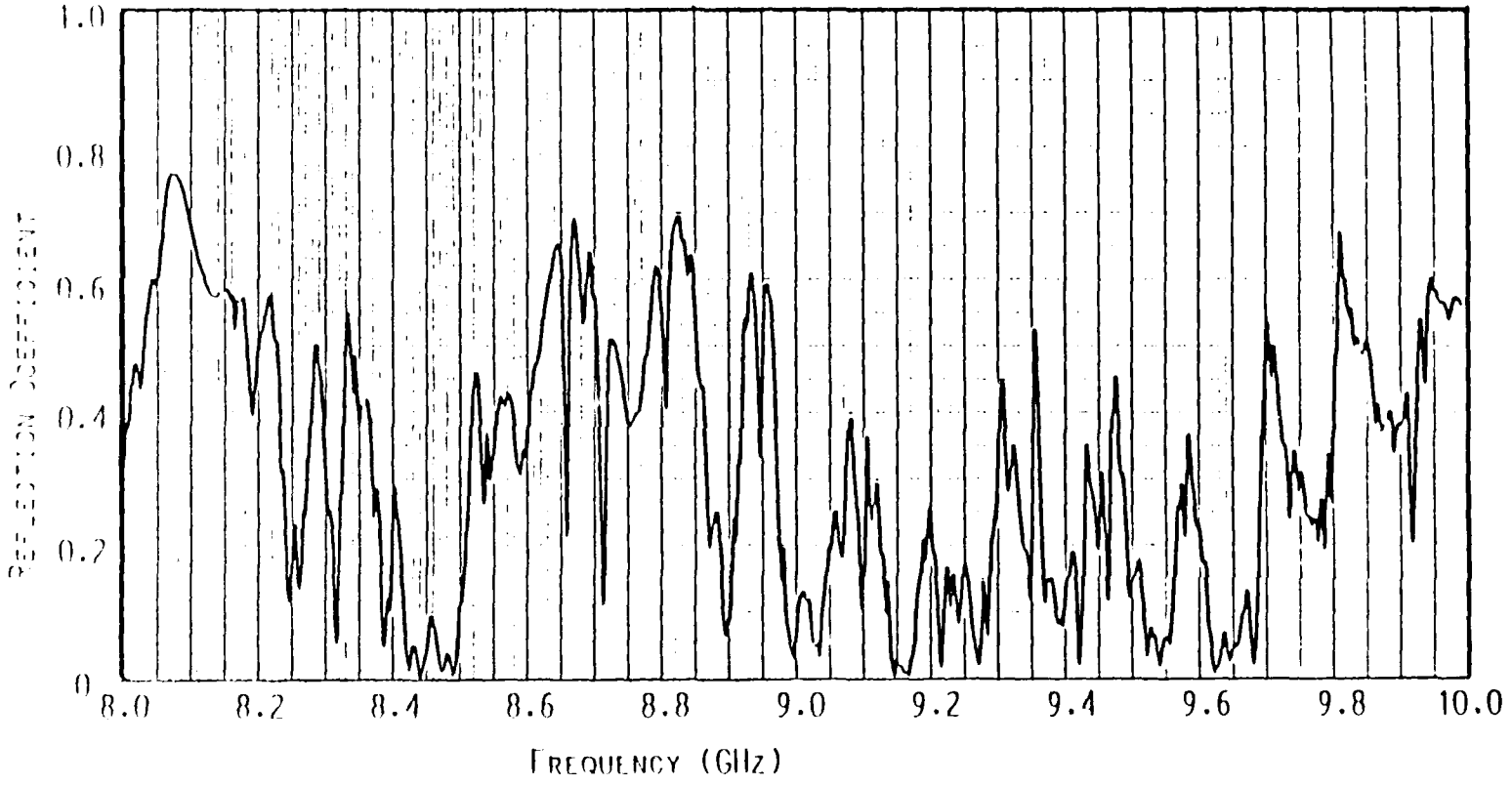

Figure 11. Reflection coefficient for pyramidal poco-graphite calorimeter.

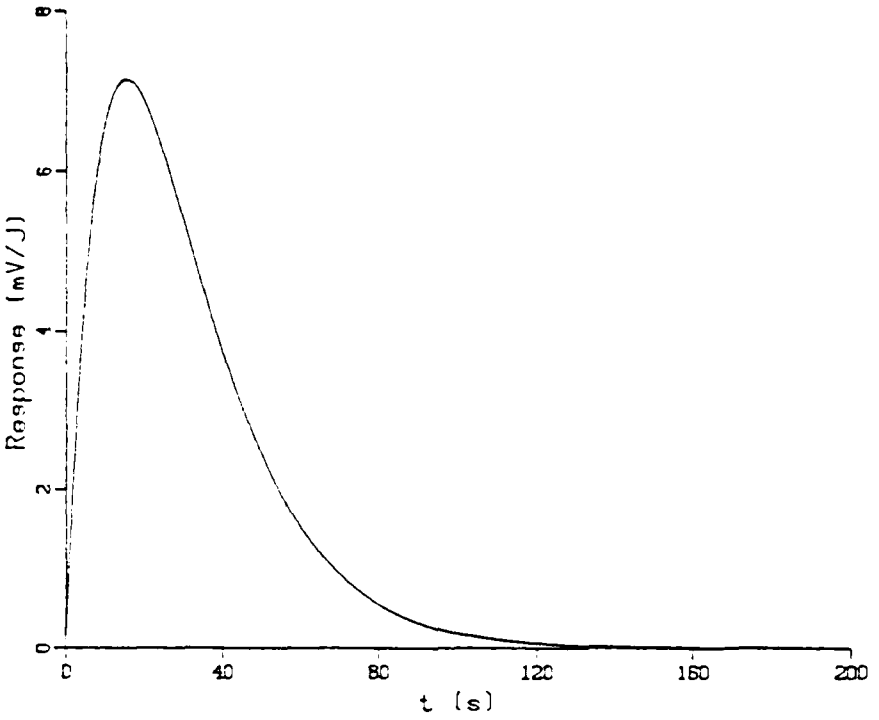

Figure 12a. Theoretical response for pyramidal poco-graphite calorimeter.

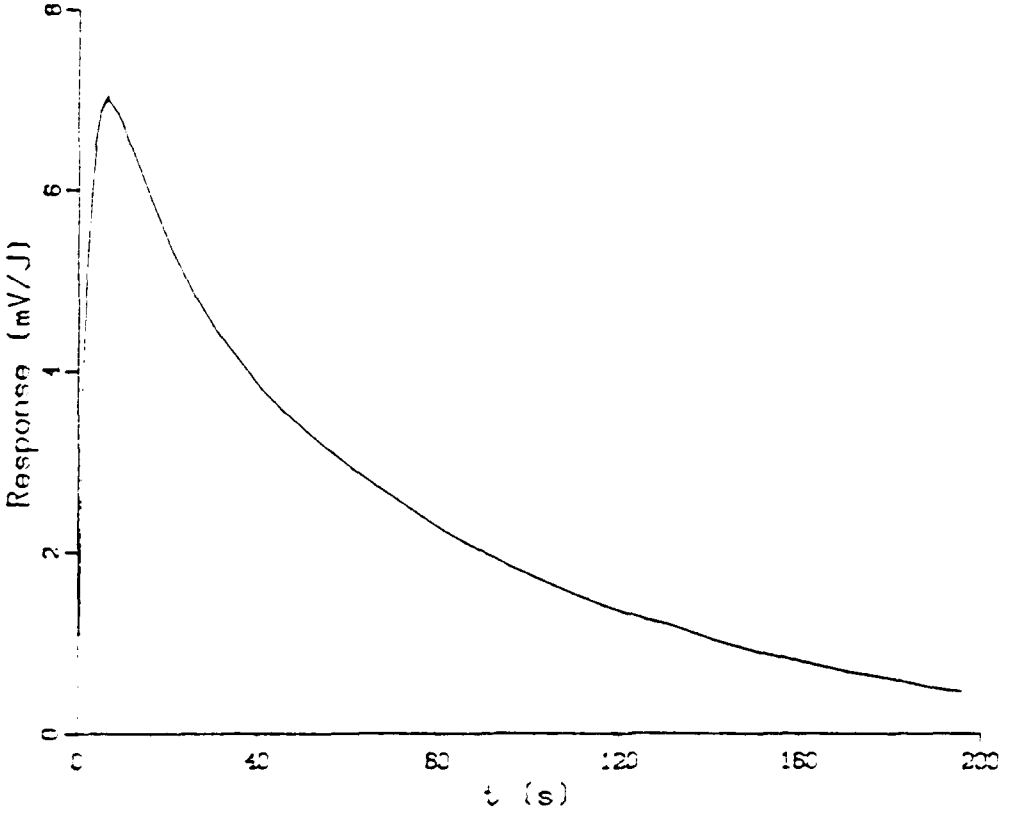

Figure 12b. Actual response for pyramidal poco-graphite calorimeter.

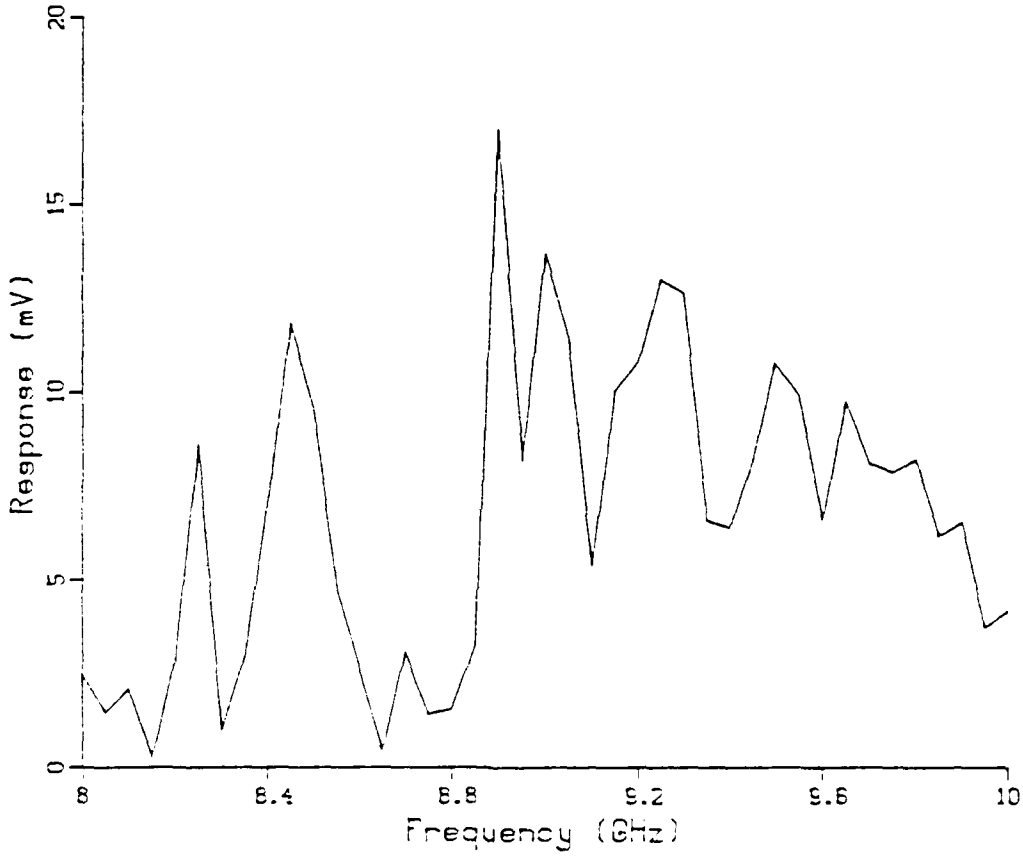

Figure 13. Response vs. frequency for pyramidal poco-graphite calorimeter.

Figure 14. The discrete points are actual data while the straight line is a least squares fit to the data with a slope of 2 mV/J. Although the last point taken was for 100 mJ, the response was quite strong and the expected minimum measurable energy is under 10 mJ.

The advantages and limitations of using calorimetric measurements for a microwave energy diagnostic are summarized below.

Advantages

1) potential broadband operation or high sensitivity

2) direct measurement

3) simple, rugged construction

4) insensitive to mode and external noise sources (x-rays, machine EMP, etc.)

5) high-power source not necessary for calibration

Limitations

1) must be designed to match well to input waveguide

2) small absorber mass necessary for detectable temperature rise

3) peak power calculated from pulse shape information

4) operation more difficult at low frequency (<4 GHz)

2.4 LEAKY-PIPE MODE SPECTROMETER.

A leaky pipe mode spectrometer makes use of the fact that different modes propagate at different speeds inside of a waveguide. Utilizing this fact in conjunction with basic antenna theory for a linear array, one can show that the angle of radiation of the array is dependent on the mode (phase velocity) (Reference 5). The leaky-pipe radiator

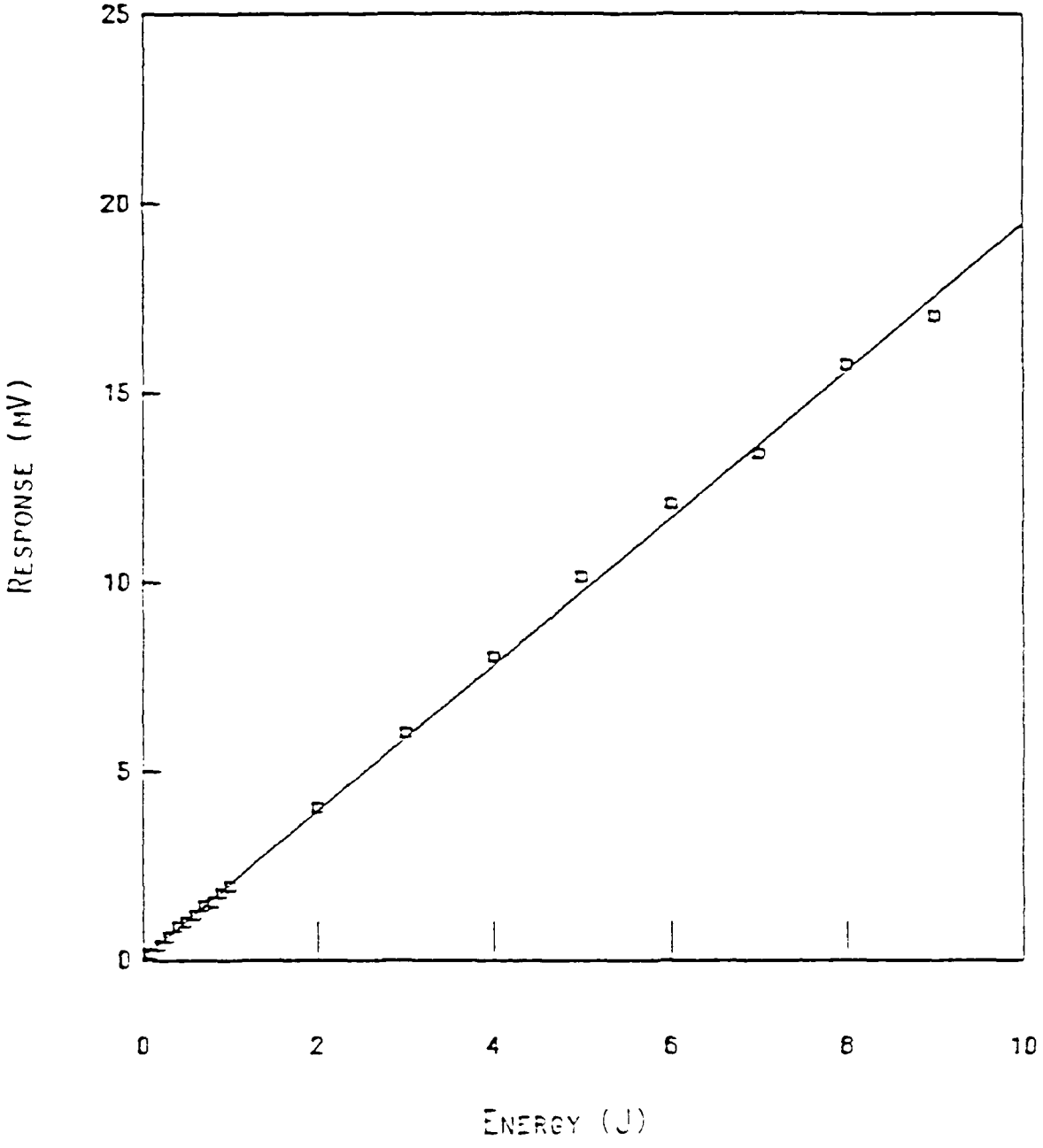

Figure 14. Response vs. input power for pyramidal poco-graphite calorimeter.

consists of a series of small apertures which radiate as a phased array. Figure 15 is a drawing of the C-band leaky-pipe radiator we utilized at PI. Figures 16 and 17 show the angular response of this device to the TE_{10} and TE_{30} modes, respectively. The TE_{30} mode was excited using a simple waveguide mode converter. Figure 18 is a plot showing the theoretical angular response of the C-band leaky-pipe radiator.

Figure 19 is a schematic drawing of a leaky-pipe radiator which shows how the radiation angle is defined. With the angle of radiation defined in this manner, the formula describing how this angle varies with frequency and mode for a TE_{mn} rectangular mode is as follows:

$$\cos\theta = \left\{1 - \left(\frac{c}{2f}\right)^2\left[\left(\frac{m}{y}\right)^2 + \left(\frac{n}{z}\right)^2\right]\right\}^{1/2} , \qquad (18)$$

where c is the speed of light, f is the frequency, y is the width of the broad side of the waveguide, and z is the width of the narrow side of the waveguide. As one can see from this formula, the angle of radiation depends on the frequency as well as the mode; however, as long as the frequency band of interest is not too large, there is sufficient separation of the modes to be able to discriminate among them.

The approach we used to map the angular pattern was to use two waveguide transducers in conjunction with the fast pulse and heterodyne detectors. This allowed us to observe how the pattern changed in time, as well as to monitor the frequency. One waveguide was left in the same position (e.g., the angle for the TE_{10} mode), and the other waveguide was moved to various angles to map the pattern.

The advantages and limitations of a leaky-pipe spectrometer to diagnose mode are summarized below.

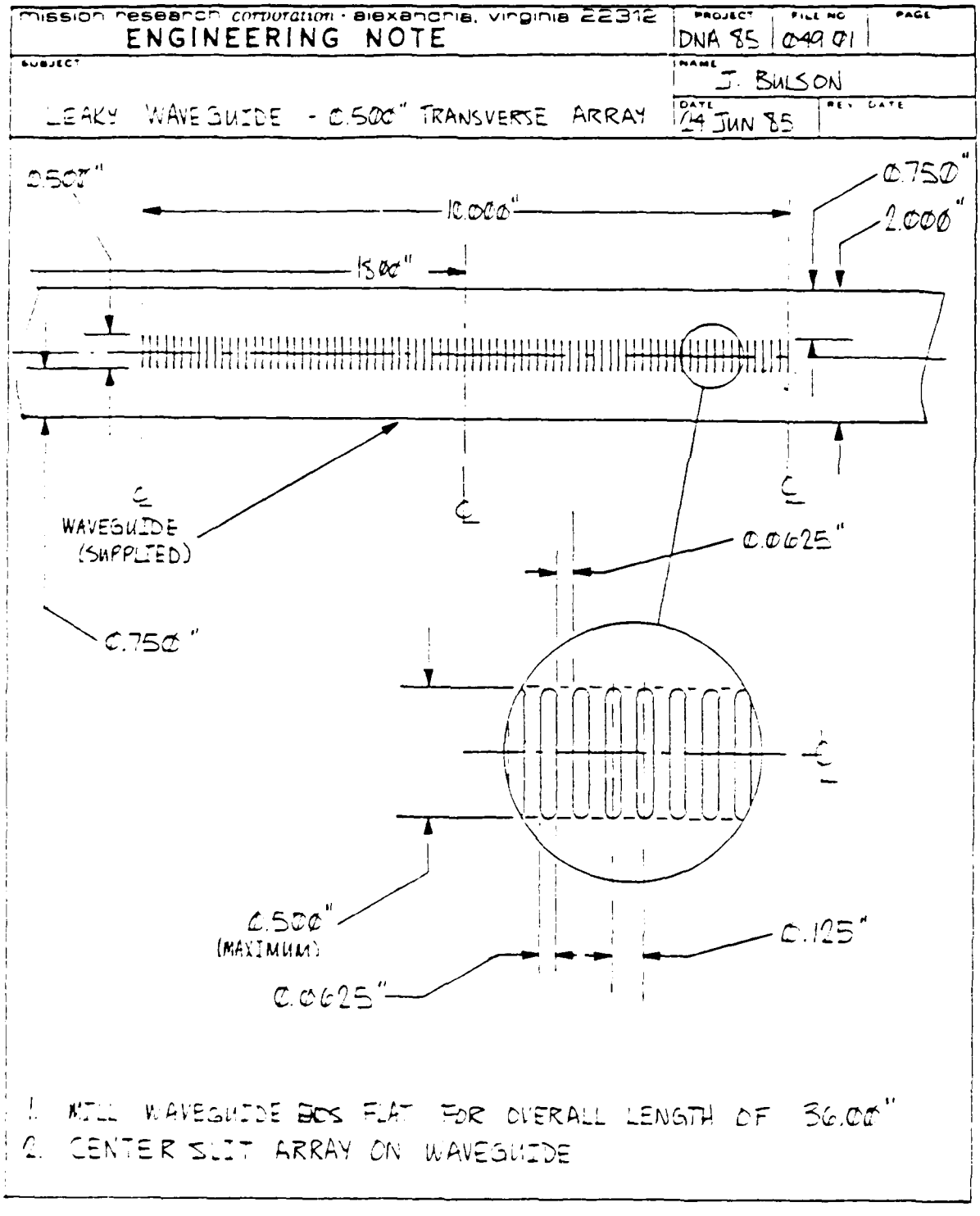

Figure 15. Mechanical drawing of C-band leaky-pipe radiator.

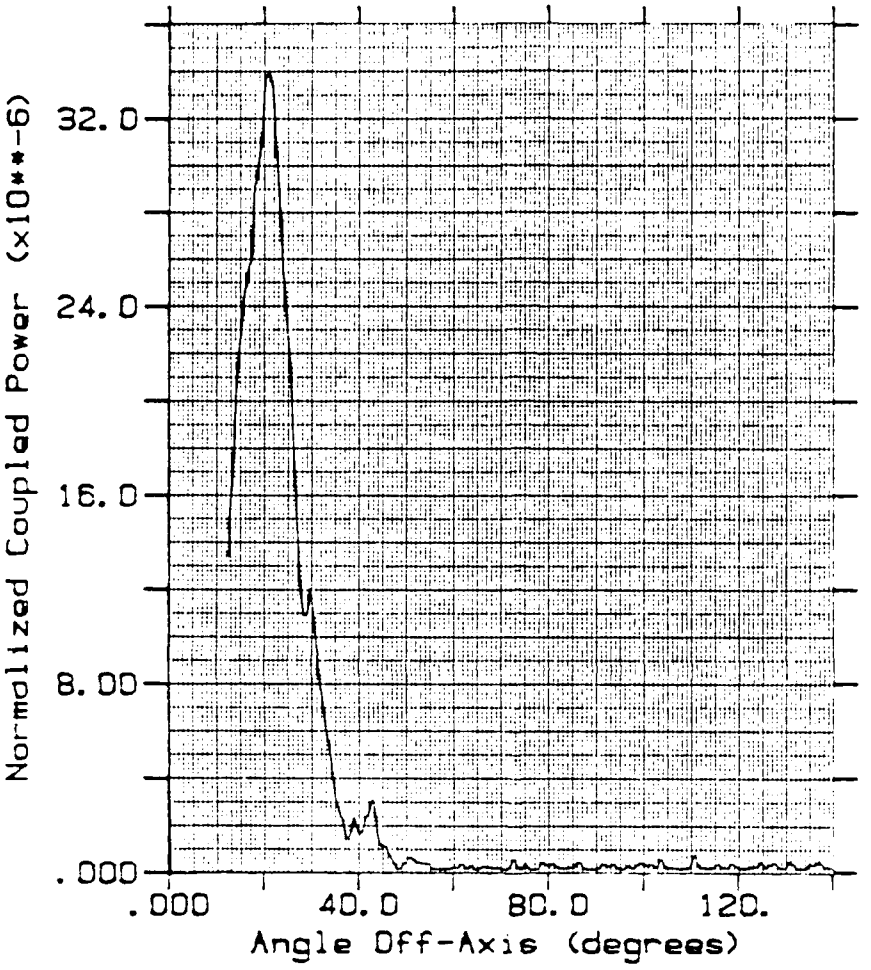

Figure 16. Angular response of C-band leaky-pipe radiator to the $TE_{..}$ mode at f = 10.5 GHz and R = 50 cm.

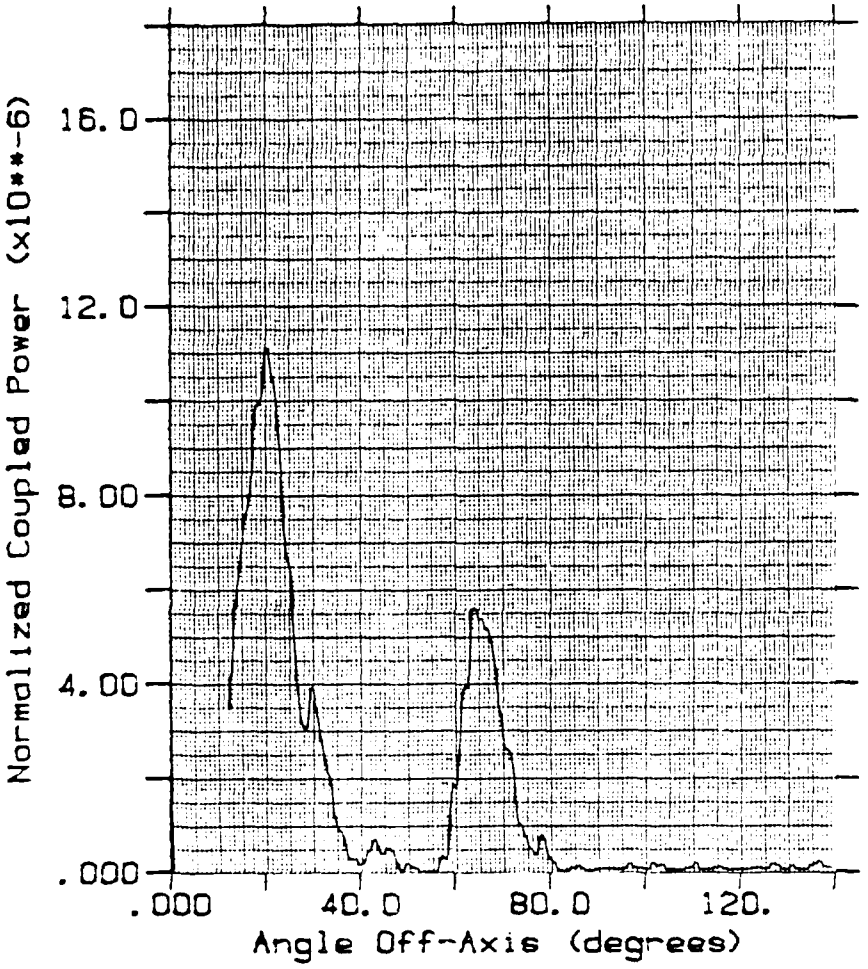

Figure 17. Angular response of C-band leaky-pipe radiator to the TE11 mode at f = 10.5 GHz and R = 80 cm.

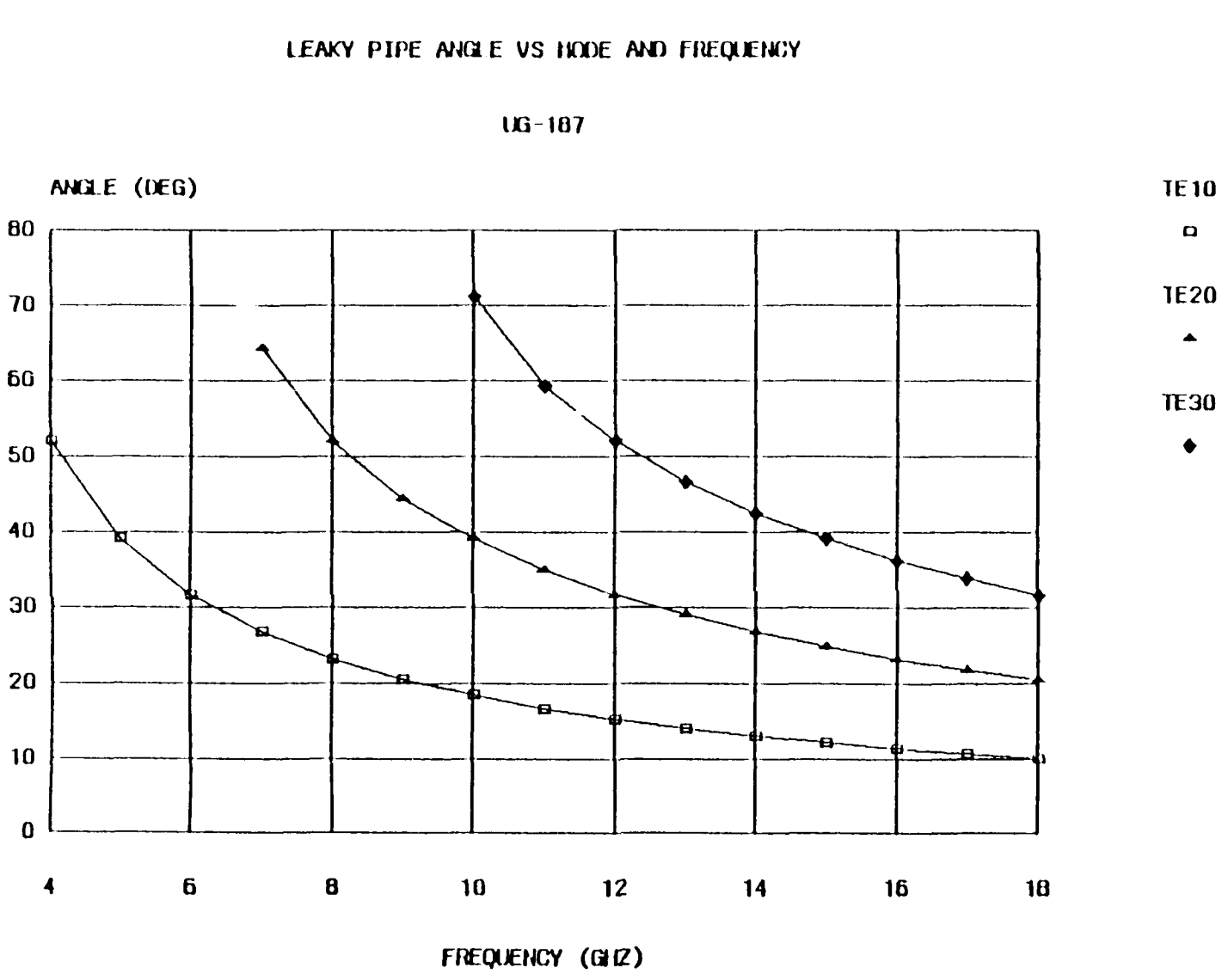

Figure 18. Theoretical angular response of C-band leaky-pipe radiator as a function of frequency for TE_{m0} modes (m = 1,2,3).

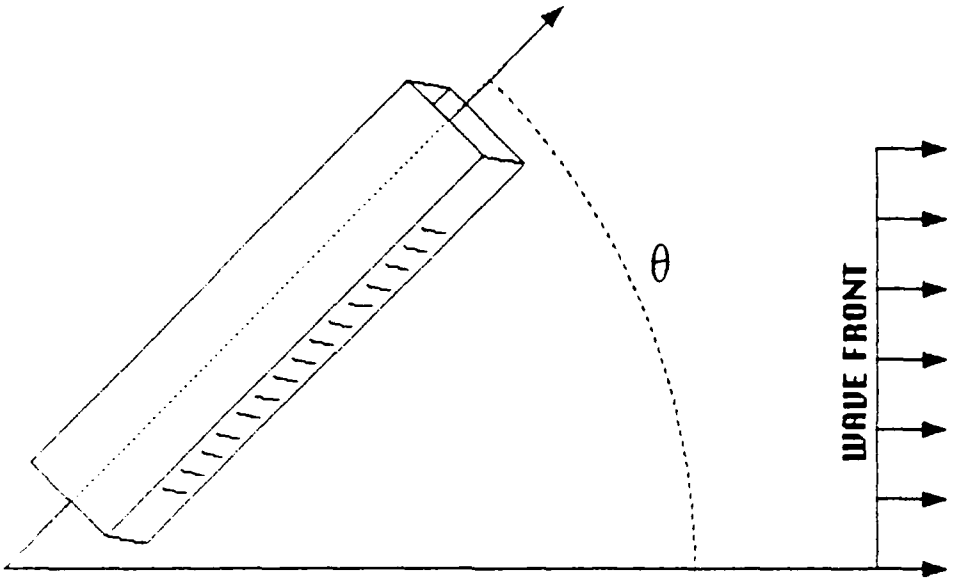

Figure 19. Schematic of a leaky-pipe spectrometer showing the angle of radiation.

Advantages

1) Simple design

2) Allows time history of the mode content to be monitored

3) Low cost

Limitations

1) Possible breakdown at radiating apertures

2) Potential for overlap of modes

SECTION 3

CROSS-CALIBRATION OF THE PI SIDE-EXTRACTION VIRCATOR

3.1 INTRODUCTION.

As a beginning to cross-calibration of the DNA HPM facilities, MRC fielded a standard diagnostic package at PI to examine the side-extraction vircator in the 8.0-12.4 GHz regime. The details of this work are described in the following sections: 3.2 Test Plan, 3.3 Microwave Pulse Shape, 3.4 Frequency Content, 3.5 Energy Content, and 3.6 Mode Content. The results may be summarized as follows:

(1) The output microwave pulse is extremely spiky in structure and not a Gaussian or rectangular shape as previously believed to be the case. The pulse consists of 2 to 5 spikes which contain greater than 50% of the total energy. These spikes generally have rise and fall times faster than 500 ps and have FWHM of approximately 1 ns. We estimate the peak power to be 1.3 GW based on crystal measurements of the microwaves radiated by the leaky pipe.

(2) The microwave output pulse appears to be approximately reproducible from shot to shot. The number of large spikes, and the relative position of the spikes is a constant. The distribution of energy in the spike may vary slightly. Thus, qualitatively the pulse shape remains the same.

(3) The frequency chirps during the pulse. There is approximately a 2 GHz range during the pulse. The frequency starts low and increases during the pulse. Changing the A-K gap changes the frequency range (as well as the pulse shape). Typical frequency data for the following A-K gaps was obtained: 1.2, 1.1, 1.0 and 0.9 cm. The

measured frequency of most of the energy for the previous A-K gaps was as follows: 8-9, 8.5-9.5, 9.5-10.5, and 10.5-11.5 GHz, respectively. Some incomplete data was also obtained at an A-K gap of 1.7 cm. The estimated frequency for this gap is 3-6 GHz.

(4) The mode of the output microwaves changes during the pulse. Tentatively, each spike appears to have a unique mode associated with it. Higher order modes occur later in time and the mode moves sequentially from the TE_{10} to the higher TE_{m0} modes. The mode content is as follows: TE_{10} (89%), TE_{20} (4%), and TE_{30} (7%), where the reference is the total time integrated energy in the pulse.

(5) Total energy in the pulse as measured using a calorimeter is 7 ± 2 joules. The uncertainty is related to the fact that the calorimeter frequency response was not as flat as originally desired. This could not be corrected in time for the PI tests and work is now underway to resolve this problem.

3.2 TEST PLAN.

Prior to performing the calibration of the PI side-extraction vircator, MRC developed a test plan which was submitted to DNA for approval and forwarded to Jim Benford at PI so that PI was aware of our test requirements. In addition to the formal test plan, correspondence with PI was carried out to assure that the PI facility was properly prepared for the MRC visit. The test plan called for two days of set-up, starting August 1, 1985, followed by nine days of operation and one day of tear down. During the nine days of testing, the following characterization of the vircator was to be performed: 1) far field measurements (all), 2) calorimetry (5.5, 11.5), 3) survey of frequency output (all), 4) survey of pulse shape (all), and 5) mode content (10.5). These measurements were to be made with the vircator configured for various frequency output in the 5-12.4 GHz regime. In the preceding list

the numbers in parenthesis indicate the microwave frequencies for which the tests were planned; "all" indicates 8.5, 9.5, 10.5, and 11.5 GHz. Additionally, we planned to examine frequency content out of band, within equipment constraints, and attempted to look at the vircator behavior as low in frequency as PI had available during our visit. Being the first users of the new PI microwave facility proved both exciting and challenging, since last minute tweaking of the facility was occurring during our test period.

As the testing began it became clear that the far field measurements needed to be expanded. This was due to the observation of a narrow, spiky structure for the pulse shape in contradiction of the original PI observations. (However, as a result of our work and implementing our diagnostic approach, PI later observed the same effect.) Further, the calorimeter testing was delayed due to damage to the calorimeter. Until PI was able to include a gate valve in the waveguide, the calorimeter was susceptible to being blown apart after each shot when the machine was vented to air to allow for rebuilding the A-K gap. We also decided to determine if it were possible to rotate the polarization of the microwaves utilizing a twist. We were able to accomplish all of the originally planned experiments, although the experimental plan itself shifted in terms of when the experiments were performed.

3.3 MICROWAVE PULSE SHAPE.

The microwave pulse shape was detected using the hybrid double-balanced mixer detectors described in Section 2.1 (homodyne detection). The rise time was limited by the bandwidth of the Tektronix 7104 oscilloscope to about 350 ps. The pulse shape for the PI side-extraction vircator was shown to be of a very spiky nature. Reproduced in Figure 20 are typical pulse shapes for four A-K gap settings of the vircator (0.9, 1.0, 1.1 and 1.2 cm). These are the A-K gap settings PI uses to cover the 8-12 GHz region. As will become obvious in

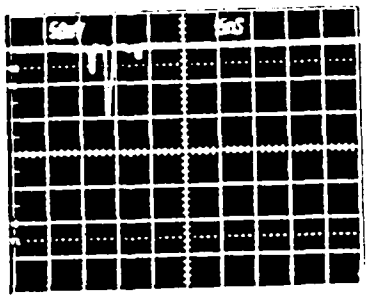

a.) Pulse Shape

for AK gap = 0.9 cm

(SHOT #8061)

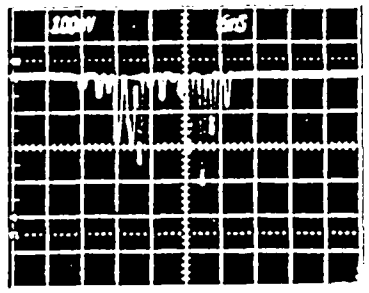

b.) Pulse Shape

for AK gap = 1.0 cm

(SHOT #8059)

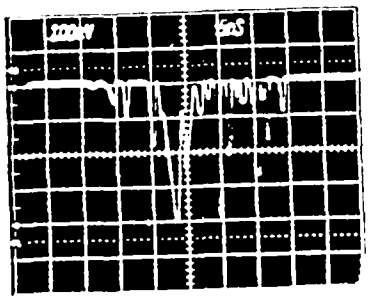

c.) Pulse Shape

for AK gap = 1.1 cm

(SHOT #8055)

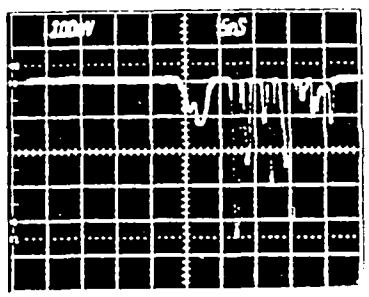

d.) Pulse Shape

for AK gap = 1.2 cm

(SHOT #8052)

Figure 20. Homodyne pulse shape measurements at turntable center for the following A-K gaps and peak powers: a) 0.9 cm, 7.4 kW/cm^2, b) 1.0 cm, 9.5 kW/cm^2, c) 1.1 cm, 11.7 kW/cm^2, d) 1.2 cm, 13.3 kW/cm^2.

the next section, the smaller the A-K gap the higher the frequency content of the pulse. The detectors operated in their linear response region, which means that the output voltage was proportional to the input power. The figures show the amplitude in mV (actual measurement) and peak power in kW/cm^2 is indicated for the largest spike. The latter is calculated based on calibrations of the mixer response as well as calibration of all attenuation in the system. This power density calculation can be in error for two reasons. There is a large amount of attenuation prior to the mixer (about 52 dB). This attenuation is made up of a number of discrete pieces, each calibrated separately. When combined, the errors in each calibration add, thus, yielding uncertainties of 1-3 dB. However, the dominant problem is that the attenuation characteristics are a function of frequency. The vircator pulse is chirping (varying in frequency) and, therefore, an estimate of an "average" attenuation must be made.

In addition to the previous four A-K gap settings, an attempt was made to examine the pulse-shape of the vircator in the S-band region. PI was exploring operation in this regime at the time of our measurement and chose an A-K gap of 1.7 cm. Our diagnostic package was not set up for this region, but we had an S-band mixer and attempted to utilize this in conjunction with some waveguide components borrowed from PI. Figure 21 shows the pulse shape (shot 8103).

Several points should be made about the previous data. First, some of the spiky structures in the figures have rise times apparently limited by the oscilloscope rise time (350 ps). Second, as the A-K gap is increased (and therefore the center frequency decreased), the rise time of the spikes decreases. Third, pulse shapes similar to the original PI pulse shapes (prior to their implementing a detection system modeled on ours), may be obtained using our detectors followed by an integrator. Figure 22 shows the output of a fast PI diode (on our recording equipment) compared to the output of our mixer detector followed by a 200 pF

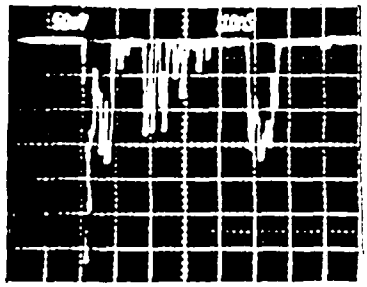

HOMODYNE

(Fast Pulse Shape Diagnostic)

Figure 21. Homodyne pulse shape measurement at turntable center for an A-K gap of 1.7 cm.

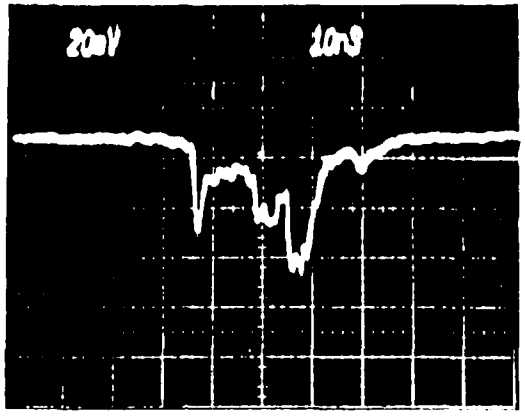

a.) PI Fast Diode

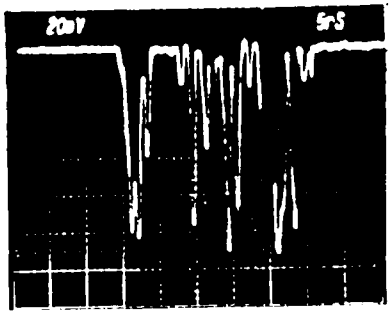

b.) HOMODYNE Pulse Shape Detector

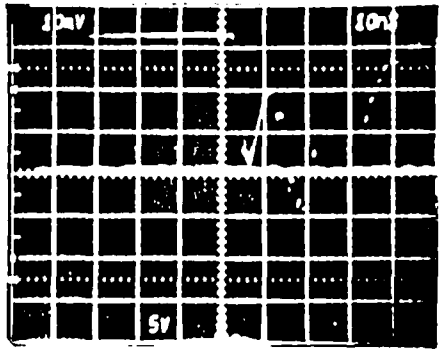

c.) HOMODYNE Pulse Shape Detector with 3 ns integrator

Figure 22. Pulse shape measurements at turntable center for an A-K gap of 1.1 cm for: a) PI fast diode on our recording equipment, b) homodyne detector, and c) homodyne detector with 3 ns integrator.

stripline integrator (shot 8069). In comparing these two outputs it should be noted that the PI crystal is operating in the square law regime, while our detector is operating in the linear regime. Thus, the PI amplitude will appear compressed compared to ours. Comparison of the ratios of the peaks in absolute units shows a strong correlation. Figure 23 shows the effect of the integrator on a fast pulse. The integration time is approximately 3 ns. Finally, the base line between gaps in the spiky data is not necessarily as flat as it appears. If the sensitivity of the detectors is increased, a small spiky structure begins to appear on the base line. This can be seen in Figure 24 (shots 8095 and 8096). The only difference between the two outputs is that 10 dB of attenuation has been removed from before the mixer detector prior to taking the second shot.

Another point to be made about the pulse shape is that it is amazingly reproducible. Thus, although the pulse shape looks different for different A-K gaps, if the A-K gap is the same the pulse shape is similar. Figure 25 shows the pulse shape for two identical sequential shots.

3.4 FREQUENCY CONTENT.

The instantaneous frequency of the microwave pulse was recorded utilizing the heterodyne approach described in Section 2.2. This technique down converts the microwave pulse and yields a signal with a frequency equal to the absolute value of $f \pm f_{LO}$, where f_{LO} is the local oscillator frequency and f is the frequency of the microwave pulse at any instant in time. The higher frequency is beyond the bandwidth of the mixer output as well as the response of our recording equipment and is not observed. Two measurements at different LO frequencies are required to determine accurately the frequency, since the down converted signal could come from either $f-f_{LO}$ or $f_{LO}-f$.

Using a splitter, the heterodyne diagnostic was used in conjunction with the pulse shape diagnostic. Thus, for each pulse shape

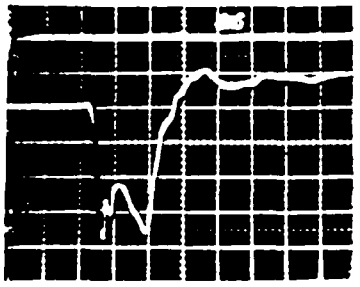

a.) Pulser Output

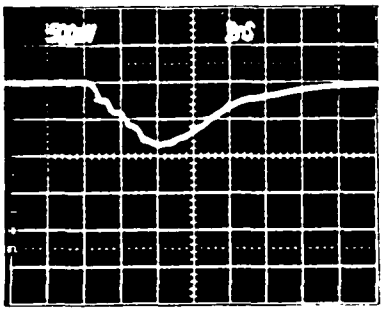

b.) Pulser Output

followed by integrator

Figure 23. Effect of integrator on fast pulse: a) pulser output with risetime of < 350 ps, b) integrated pulser output with risetime of 3 ns. Both signals were recorded on TEK7104/7A29 scopes.

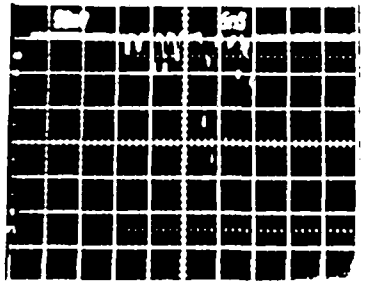

a.) HOMODYNE Pulse Shape Detector with normal attenuation

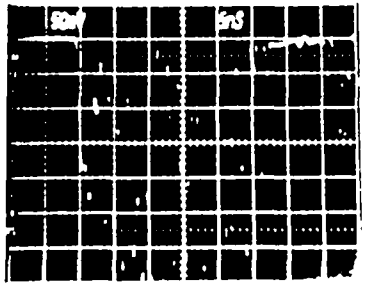

b.) HOMODYNE Pulse Shape Detector with 10 dB Attenuation removed

Figure 24. Homodyne pulse shape measurements at turntable center for an A-K gap of 1.0 cm showing baseline power level: a) attenuation = 37 dB, b) Attenuation 27 dB.

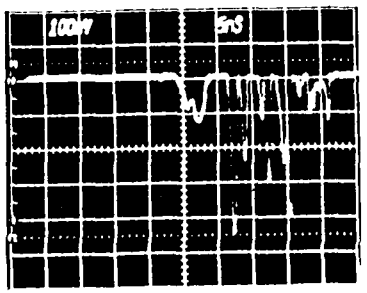

a.) Pulse Shape

for AK gap = 1.2 cm

(SHOT #8052)

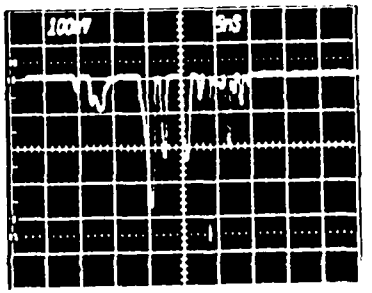

b.) Pulse Shape

for AK gap = 1.2 cm

(SHOT #8053)

Figure 25. Homodyne pulse shape measurements at turntable center for an A-K gap of 1.2 cm showing pulse shape reproducibility: a) shot #8052, b) shot #8053.

output there is a corresponding heterodyne output. Figure 26 shows the corresponding heterodyne outputs for the previous pulse shape data (Figure 20) and corresponds to the vircator A-K gap set at 0.9, 1.0, 1.1, and 1.2 cm. Examination of the figures shows a pulse with high frequency followed by lower frequency followed by higher frequency. This is because the frequency is increasing in time and the local oscillator frequency has been set approximately in the middle of the frequency band. Thus, initially the heterodyne signal is f_{LO}-f and ends up being f-f_{LO} passing through zero ($f=f_{LO}$). The amplitude of the heterodyne signal is not significantly modulated by the pulse shape because the detector is operated in the saturated, nonlinear regime. However, some amplitude modulation is apparent in Figure 26c. The instantaneous frequency can be calculated from Figure 26 using the LO frequency given and knowing that the frequency chirps from low to high.

3.5 ENERGY CONTENT.

The energy of the microwave pulse was measured with a calorimeter. The PI L-band waveguide was tapered down to C-band waveguide and an absorbing cone monitored by thermistors collected the energy. The calorimeter was described in Section 2.3. The major difficulty we encountered with the calorimeter was damage to the absorbing cone. When the tests were first begun, the calorimeter had to be vented to air from vacuum every time the vircator came up to air pressure. This occurred after each shot so that the A-K gap could be rebuilt. The burst of air coming down the waveguide blew the cone apart even though care was taken to let the pressure up slowly. With the addition of a waveguide gate valve between the vircator and the calorimeter this problem was alleviated. The valve was installed for shot 5070 and all succeeding shots.

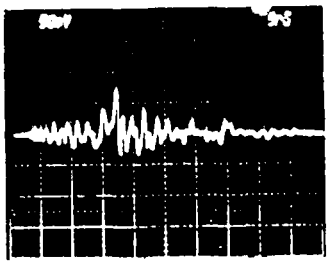

a.) Heterodyne Signal

for AK gap = 0.9 cm

(SHOT #8061)

f(LO) = 10.5 GHz

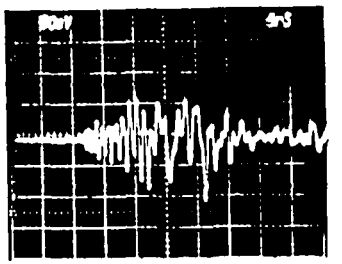

b.) Heterodyne Signal

for AK gap = 1.0 cm

(SHOT #8059)

f(LO) = 10.0 GHz

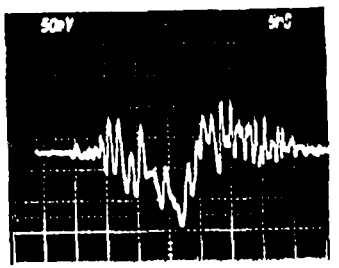

c.) Heterodyne Signal

for AK gap = 1.1 cm

(SHOT #8055)

f(LO) = 9.0 GHz

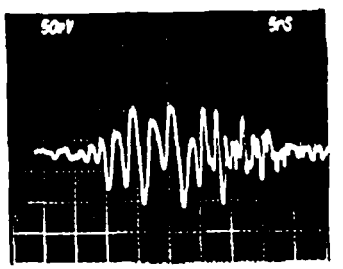

d.) Heterodyne Signal

for AK gap = 1.2 cm

(SHOT #8052)

f(LO) = 8.5 GHz

Figure 26. Heterodyne frequency measurements at turntable center for the following A-K gaps: a) 0.9 cm, b) 1.0 cm, c) 1.1 cm, and d) 1.2 cm.

A summary of the calorimeter data is shown in Table 2 and a typical response is shown in Figure 27. The table lists only those shots where calorimeter data was analyzable. Some shots resulted in poor calorimeter response for various reasons which will be discussed below. For an A-K gap of 1.1 cm, the first shot (#8062) resulted in the only measurement that we report with confidence: 7.2 ± 2.5 joules. Preparations for the subsequent shot damaged the cone, resulting in poor response for the succeeding shots with cone B. Subsequent shots with the calorimeter also included the 1" leaky-pipe spectrometer, with the exception of shots 8086-8089. The total power coupled to free space by the leaky-pipe is unknown, and hence the fraction of the power detected by the calorimeter is unknown. It is known, however, that the fractional coupled power is quite significant. The measurements of the energy, from shot to shot, are consistent, however. For A-K gaps of 1.0 cm and 1.2 cm, the average detected energy is 0.56 ± 0.20 joules and 0.28 ± 0.09 joules, respectively. When the leaky-pipe was removed, the energy measurements did not change significantly. This may be attributed to possible breakdown across the mylar window which was in place to protect the detecting cone from remnants of the exploding cathode. The response shown in Figure 27 is raw data for shot 8062. Time proceeds from right to left. The data was analyzed by extrapolating to t = 0 and referring to the calibration factor (in joules/mV) for heterodyne measured average frequency for that shot.

3.6 MODE CONTENT.

The mode content of the vircator microwave pulse was measured utilizing the leaky-pipe approach described in Section 2.4. The leaky-pipe was constructed from C-band waveguide and consisted of 81 slots, 2.54 cm long, and 0.1588 cm wide oriented perpendicular to the direction of propagation along the broadwall. A 1.27 cm thick plexiglass window utilized an O-ring to maintain vacuum integrity. The same taper used with the calorimeter, from L-band to C-band, was required in order to

Table 2. Summary of PI Vircator Calorimetric Measurements.

SHOT#	A-K GAP (cm)	ENERGY (Joules)	CONE#	NOTES
8078	1.0	0.688 ± 0.243	C	LP,MY
8079	1.0	0.331 ± 0.117	C	LP,MY
8080	1.0	0.666 ± 0.235	C	LP,MY
8087	1.0	0.527 ± 0.186	C	MY
8089	1.0	0.718 ± 0.253	C	MY
8062	1.1	7.19 ± 2.53	B	EB
8064	1.1	2.05 ± 0.72	B	EB,DA
8071	1.1	0.239 ± 0.084	C	LP,EB
8075	1.1	1.92 ± 0.677	C	LP,MY
8076	1.1	0.230 ± 0.081	C	LP,MY
8081	1.2	0.244 ± 0.086	C	LP,MY
8082	1.2	0.206 ± 0.073	C	LP,MY
8083	1.2	0.206 ± 0.073	C	LP,MY
8084	1.2	0.422 ± 0.149	C	LP,MY
8085	1.2	0.297 ± 0.105	C	LP,MY
8086	1.2	0.527 ± 0.186	C	MY

EB = E-Bend
LP = Leaky-Pipe
MY = Mylar
DA = Damaged

Note: All diagnostic configurations include an L-band to C-band adapter as the first element and the calorimeter as the last element.

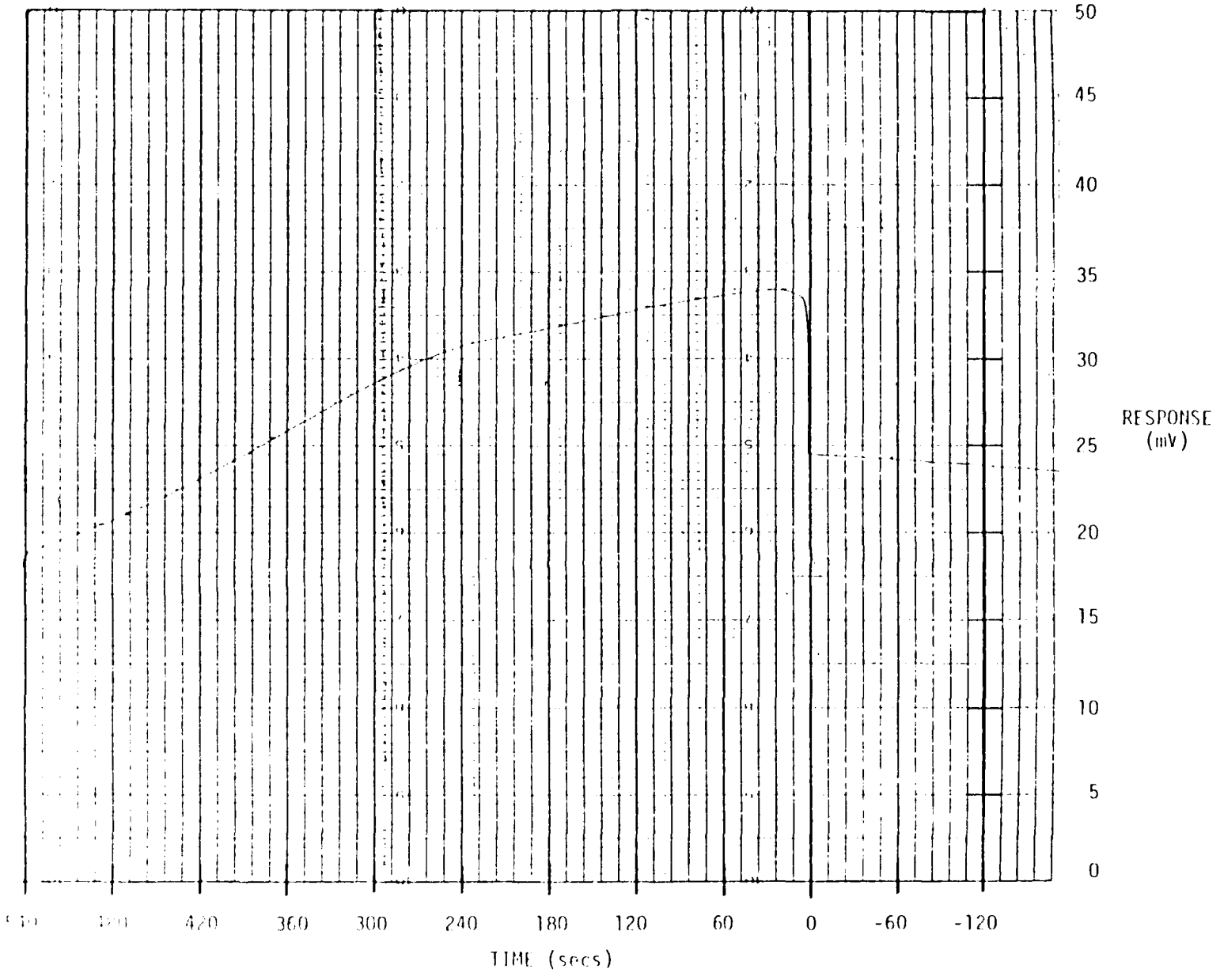

Figure 27. Typical calorimetric energy measurement of the PI vircator for an A-K gap of 1.1 cm with the response showing an energy of 7 ± 2 joules.

mate the leaky-pipe to the vircator. The angular pattern from the leaky-pipe was monitored for an A-K gap of 1.0, 1.1, and 1.2 cm. The pulse shape for three A-K gaps was monitored at the following three angles from the leaky-pipe axis: 20°, 45°, and 65°. These are the approximate angular positions of the TE_{10}, TE_{20}, and TE_{30} modes, respectively, at 9 GHz. Then, utilizing the theoretically calculated angular response versus mode, an identification of modes was made. We assumed that the leaky-pipe radiated uniformly for the modes of interest. This is a reasonable assumption given the construction of our leaky-pipe for TE_{m0} modes. Representative data is shown in Figures 28-30 for A-K gaps of 1.0, 1.1, and 1.2 cm, respectively.

The analysis of the data shows that the vircator has an amazingly pure modal spectrum given the over-moded nature of its output waveguide. Eighty-nine per cent of the energy is in the TE_{10} mode in the waveguide with about 4% in the TE_{20} mode and 7% in the TE_{30} mode. It is not surprising that more energy is in the TE_{30} mode since this mode is more easily excited by the vircator than the TE_{20} mode.

3.7 CONCLUSIONS.

The calibration of the PI side-extraction vircator was successful. It was the first experimental indication that vircators generate microwave energy in sharp bursts. Although the pulse shape data was different (spiky) than originally reported, the energy content was similar to that reported. This is due to the integrating nature of the diagnostics PI had been using. Thus, the energy content, which was suspected of being the key factor in the system and component failure, was as expected. The vircator pulse is not ideal for HPM testing. It does not have uniform amplitude, but more important, the energy per frequency content is low since the frequency is continuously changing. In its defense, it does expose targets to a broad range of frequencies.

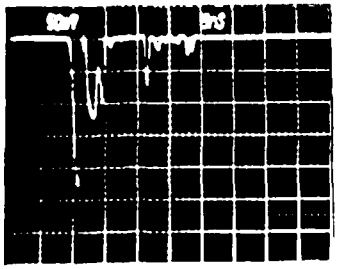

a.) Pulse Shape

for AK gap = 1.0 cm, θ = 20°

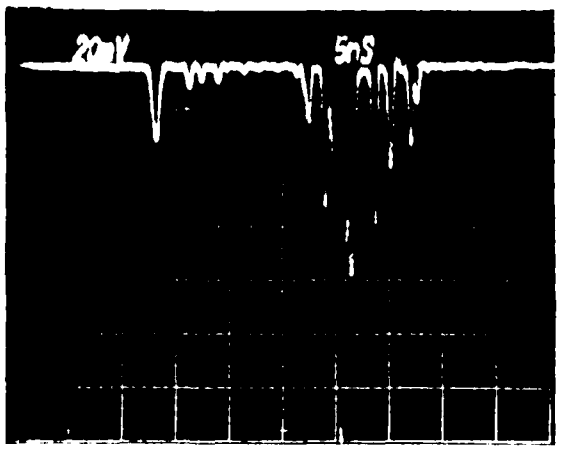

b.) Pulse Shape

for AK gap = 1.0 cm, θ = 44.5°

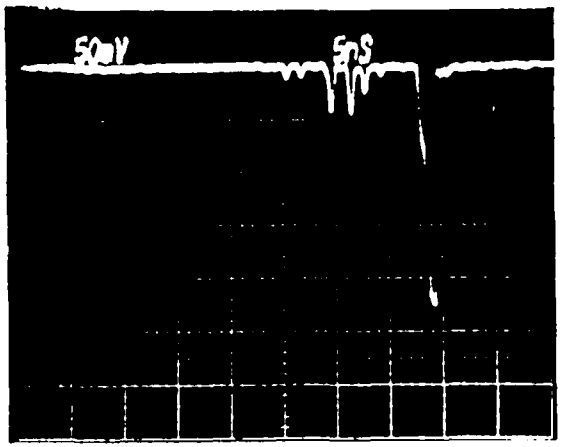

c.) Pulse Shape

for AK gap = 1.0 cm, θ = 65°

Figure 28. Homodyne pulse shape measurements at three angles from leaky-pipe axis for an A-K gap of 1.0 cm: a) θ = 20°, b) θ = 45.5°, c) θ = 65°, corresponding to the TE_{10} mode, TE_{20} mode, and TE_{30} mode, respectively.

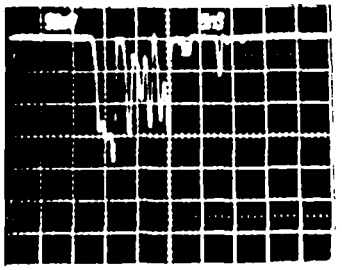

a.) Pulse Shape

for AK gap = 1.1 cm, θ = 20.5°

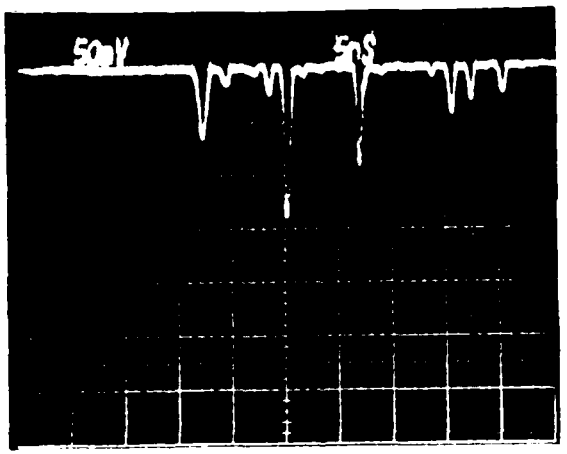

b.) Pulse Shape

for AK gap = 1.1 cm, θ = 44.5°

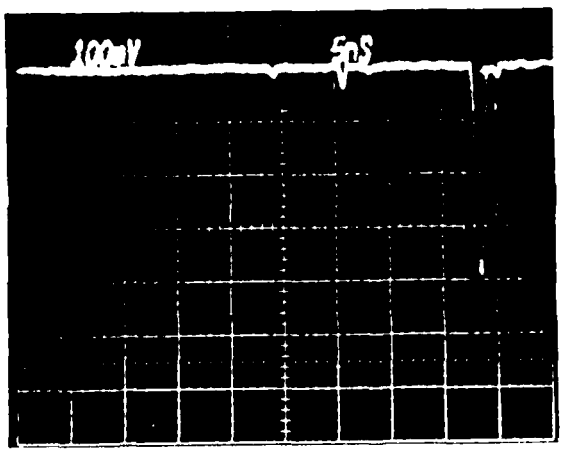

c.) Pulse Shape

for AK gap = 1.1 cm, θ = 64.5°

Figure 29. Homodyne pulse shape measurements at three angles from leaky-pipe axis for an A-K gap of 1.1 cm: a) θ = 20.5°, b) θ = 44.5°, c) θ = 64.5°, corresponding to the TE_{10} mode, TE_{20} mode, and TE_{30} mode, respectively.

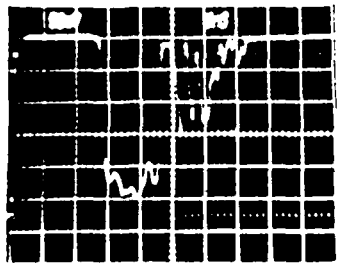

a.) Pulse Shape

for AK gap = 1.2 cm. θ = 20°

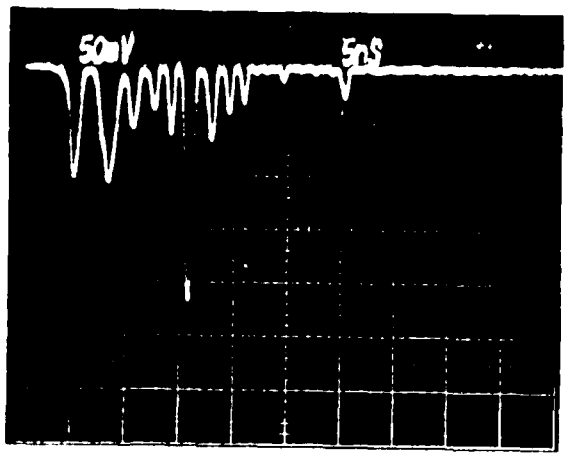

b.) Pulse Shape

for AK gap = 1.2 cm. θ = 44.5°

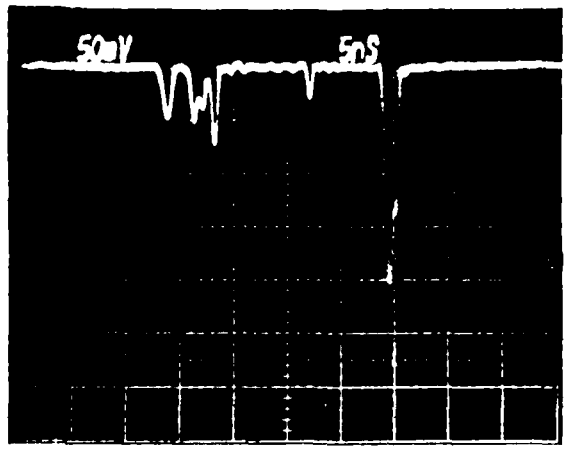

c.) Pulse Shape

for AK gap = 1.2 cm. θ = 65°

Figure 30. Homodyne pulse shape measurements at three angles from leaky-pipe axis for an A-K gap of 1.2 cm: a) θ = 20°, b) θ = 44.5°, c) θ = 64°, corresponding to the TE_{10} mode, TE_{20} mode, and TE_{30} mode, respectively.

The diagnostics MRC fielded in this work were, in general, source diagnostics. Thus, the leaky-pipe and the calorimeter diagnostics focused on the source and not the radiated field. Some field mapping was performed, but was limited by the number of recording channels. It is our recommendation that a multichannel field mapping capability be developed. This would allow the radiated field, which is to be used by testers, to be measured directly.

SECTION 4

LIST OF REFERENCES

1. "Diagnostic Package Update," DNA High-Power Microwave Technical Review Proceedings, July 1985.

2. "Microwave Detecting Diode Rise-Time Measurements," Rev. Sci. Instrum., 1985.

3. "Front-End Components for Submillimeter-Wave Schottky-Diode Receivers," IEEE International Conference on Infrared and Millimeter Waves, 1985.

4. R. R. Bartsch, private communication.

5. Principles and Applications of Waveguide Transmission, Van Nostrand, 1950.

DISTRIBUTION LIST

DEPARTMENT OF DEFENSE

ASSISTANT SECRETARY OF DEFENSE
CMD, CONTROL, COMMUNICATIONS & INTEL
ATTN: DASD(C3)
ATTN: DASD(I)
ATTN: DASD(P&R)

ASSISTANT TO THE SECRETARY OF DEFENSE
ATTN: EXECUTIVE ASSISTANT

DEFENSE ADVANCED RSCH PROJ AGENCY
ATTN: DED

DEFENSE COMMUNICATIONS AGENCY
ATTN: CODE H396 TECH LIB

DEFENSE INTELLIGENCE AGENCY
ATTN: DT(SCI-TECH INTELL)
ATTN: DT-4C (DR J COLEMAN)
ATTN: RTS-2A (TECH LIB)
ATTN: RTS-2B

DEFENSE NUCLEAR AGENCY
ATTN: DFRA
ATTN: RAEV
4 CYS ATTN: TITL

DEFENSE TECHNICAL INFORMATION CENTER
12CYS ATTN: DD

FIELD COMMAND DEFENSE NUCLEAR AGENCY
ATTN: FTTD

FIELD COMMAND/DNA
ATTN: FC-1

NATIONAL SECURITY AGENCY
ATTN: TECHNICAL LIBRARY

STRATEGIC DEFENSE INITIATIVE ORGANIZATION
ATTN: T/SL

UNDER SECRETARY OF DEFENSE
ATTN: DEP UND SEC C3I-STRAT/THEA C2 SYS
ATTN: DEP UND SEC RES & ADV TECH
ATTN: DEP UND SEC/TAC WARFARE PROG
ATTN: STRAT & SPACE SYS(OS)
ATTN: STRAT & THEATER NUC FORCES

DEPARTMENT OF THE ARMY

DEPARTMENT OF THE ARMY
ATTN: DAMO TCV A

HARRY DIAMOND LABORATORIES
ATTN: SCHLD-NW-P
ATTN: SLCHD-NE-EB
ATTN: SLCHD-NW
2 CYS ATTN: SLCHD-NW-E
ATTN: SLCHD-NW-EC
ATTN: SLCHD-NW-ED
ATTN: SLCHD-NW-EE
ATTN: SLCHD-NW-R
ATTN: SLCHD-NW-RA
ATTN: SLCHD-NW-RC
ATTN: SLCHD-NW-RE
ATTN: SLCHD-NW-RH G MERKEL
ATTN: SLCHD-NW-RH R GILBERT
ATTN: SLCHD-NW-RI G HUTTLIN
ATTN: SLCIS-IM-TL (TECH LIB)

RESEARCH & DEV CENTER
ATTN: DRCPM-TDS-SD

U S ARMY ARMAMENT RSCH & DEV CENTER
ATTN: TECHNICAL LIBRARY

U S ARMY ARMOR CENTER
ATTN: TECHNICAL LIBRARY

U S ARMY BALLISTIC RESEARCH LAB
ATTN: SLCBR-SS-T (TECH LIB)
ATTN: SLCBR-VL-LD

U S ARMY BELVOIR RD & E CTR
ATTN: TECH LIB

U S ARMY COMBINED ARMS CENTER
ATTN: TECHNICAL LIBARY

U S ARMY FOREIGN SCIENCE & TECH CTR
ATTN: DRXST-PO T CALDWELL

U S ARMY MISSILE COMMAND
ATTN: TECH LIBRARY

U S ARMY TEST AND EVALUATION COMD
ATTN: TECHNICAL LIBRARY SI F

U S ARMY VULNERABILITY ASSESSMENT LAB
ATTN: SLCVA-TAC (R FLONSS)

DEPARTMENT OF THE NAVY

NAVAL AIR SYSTEMS COMMAND
ATTN: AIR 5161
ATTN: AIR 5164
ATTN: AIR 5462
ATTN: AIR 933

NAVAL INTELLIGENCE SUPPORT CTR
ATTN: DE0O
ATTN: LIBRARY

NAVAL POSTGRADUATE SCHOOL
ATTN: CODE 1424 LIBRARY

NAVAL RESEARCH LABORATORY
ATTN: CODE 2627 (TECH LIB)
ATTN: CODE 4000 W ELLIS
ATTN: CODE 4607 (S BABJAK)
ATTN: CODE 4700 1 (W ALI)
ATTN: CODE 4741 (A FLIFET)
ATTN: CODE 8320 1 (V FOLEN)

NAVAL SURFACE WEAPONS CENTER
ATTN: R RICHARDSON
ATTN: TECH LIBRARY & INFO SVCS BR

OFC OF THE DEPUTY CHIEF OF NAVAL OPS
ATTN: NOP 506
ATTN: NOP 94
ATTN: NOP 982
ATTN: NOP 987
ATTN: NOP 956
ATTN: OP 981

SPACE & NAVAL WARFARE SYSTEMS CMD
ATTN: PMW 145

DEPARTMENT OF THE AIR FORCE

AF INE
ATTN: INET

AIR FORCE ELECTRONIC WARFARE CENTER
ATTN: TECHNICAL LIBARY

AIR FORCE INSTITUTE OF TECHNOLOGY/EN
ATTN: ENA: MAJ D STONE

AIR FORCE SYSTEMS COMMAND
ATTN: DLWW

AIR FORCE WEAPONS LABORATORY
ATTN: AWP
ATTN: AWPB
ATTN: NT
ATTN: NTCA B SINGARAJU

BALLISTIC MISSILE OFFICE
ATTN: MYSP

ELECTRONIC SYSTEMS DIVISION/SC
ATTN: SCS 1E
ATTN: TECHNICAL LIBRARY

FOREIGN TECHNOLOGY DIVISION, AFSC
ATTN: LIBRARY

ROME AIR DEVELOPMENT CENTER, AFSC
ATTN: RBCM
ATTN: RBCT

SPACE DIVISION/YA
ATTN: YAR

DEPARTMENT OF ENERGY

LAWRENCE LIVERMORE NATIONAL LAB
ATTN: L-156
ATTN: L-53 TECH INFO DEPT LIBRARY

LOS ALAMOS NATIONAL LABORATORY
ATTN: MS D408
ATTN: MS F617
ATTN: MS H827
ATTN: REPORT LIBRARY

SANDIA NATIONAL LABORATORIES
ATTN: DEPT 1230
ATTN: DEPT 1235
ATTN: DEPT 7555
ATTN: TECH LIB 3141 (RPTS REC CLRK)

OTHER GOVERNMENT

CENTRAL INTELLIGENCE AGENCY
ATTN: OSR/SE/C
ATTN: OSR/SE/F
ATTN: OSWR/NED
ATTN: OSWR/SSD/SWB
ATTN: OSWR/STD/TTB

DEPARTMENT OF DEFENSE CONTRACTORS

BATTELLE MEMORIAL INSTITUTE
ATTN: ELEC SYS DEPT/V PUBLIELLI

GENERAL DYNAMICS CORP
ATTN: TECHNICAL LIBRARY

HUGHES AIRCRAFT CO
ATTN: G SARAN

JAYCOR
ATTN: E WENAAS

JAYCOR
ATTN: R BONN

KAMAN SCIENCES CORP
ATTN: K LEE

KAMAN SCIENCES CORP
ATTN: C EKLUND
ATTN: LIBRARY B KINGLOW

KAMAN SCIENCES CORP
ATTN: E CONRAD

KAMAN SCIENCES CORPORATION
ATTN: DASIAC

KAMAN TEMPO
ATTN: DASIAC
ATTN: R RUTHERFORD

MAXWELL LABS, INC
ATTN: TECHNICAL LIBARY

MISSION RESEARCH CORP
ATTN: D SULLIVAN

MISSION RESEARCH CORP
2 CYS ATTN: J M BULSON
2 CYS ATTN: M BOLLEN

MITRE CORPORATION
ATTN: TECHNICAL REPORT CENTER

PACIFIC SIERRA RESEARCH CORP
ATTN: H BRODE, CHAIRMAN SAGE
ATTN: L E JOHNSON

PHYSICS INTERNATIONAL CO
ATTN: DOCUMENT CONTROL
ATTN: J BENFORD

PULSE SCIENCES, INC
ATTN: TECHNICAL LIBARY

R & D ASSOCIATES
ATTN: DOCUMENT CONTROL
ATTN: W KARZAS

R & D ASSOCIATES
ATTN: R PARKER

ROCKWELL INTERNATIONAL CORP
ATTN: TECHNICAL LIBRARY

SCIENCE APPLICATIONS INTL CORP
ATTN: TECH LIBRARY

SRI INTERNATIONAL
ATTN: ELECTROMAG SCI LAB TECH LIB

TRW INC
ATTN: P BHUTA

VARIAN ASSOCIATES INC
ATTN: TECHNICAL LIBRARY

WESTINGHOUSE ELECTRIC CORP
ATTN: TECHNICAL LIBRARY

END

DATE

FILMED

5-88

DTIC